AD-A107 939 HERIOT-WATT UNIV EDINBURGH (SCOTLAND) DEPT OF PHYSICS F/G 20/5
SUBMILLIMETER LASER AND FABRY-PEROT SPECTROSCOPY USING METALLIC--ETC(U)
MAY 81 C R PIDGEON, B W DAVIS DA-ERO-78-G-074

UNCLASSIFIED NL

END
DATE FILMED
1 82
DTIC

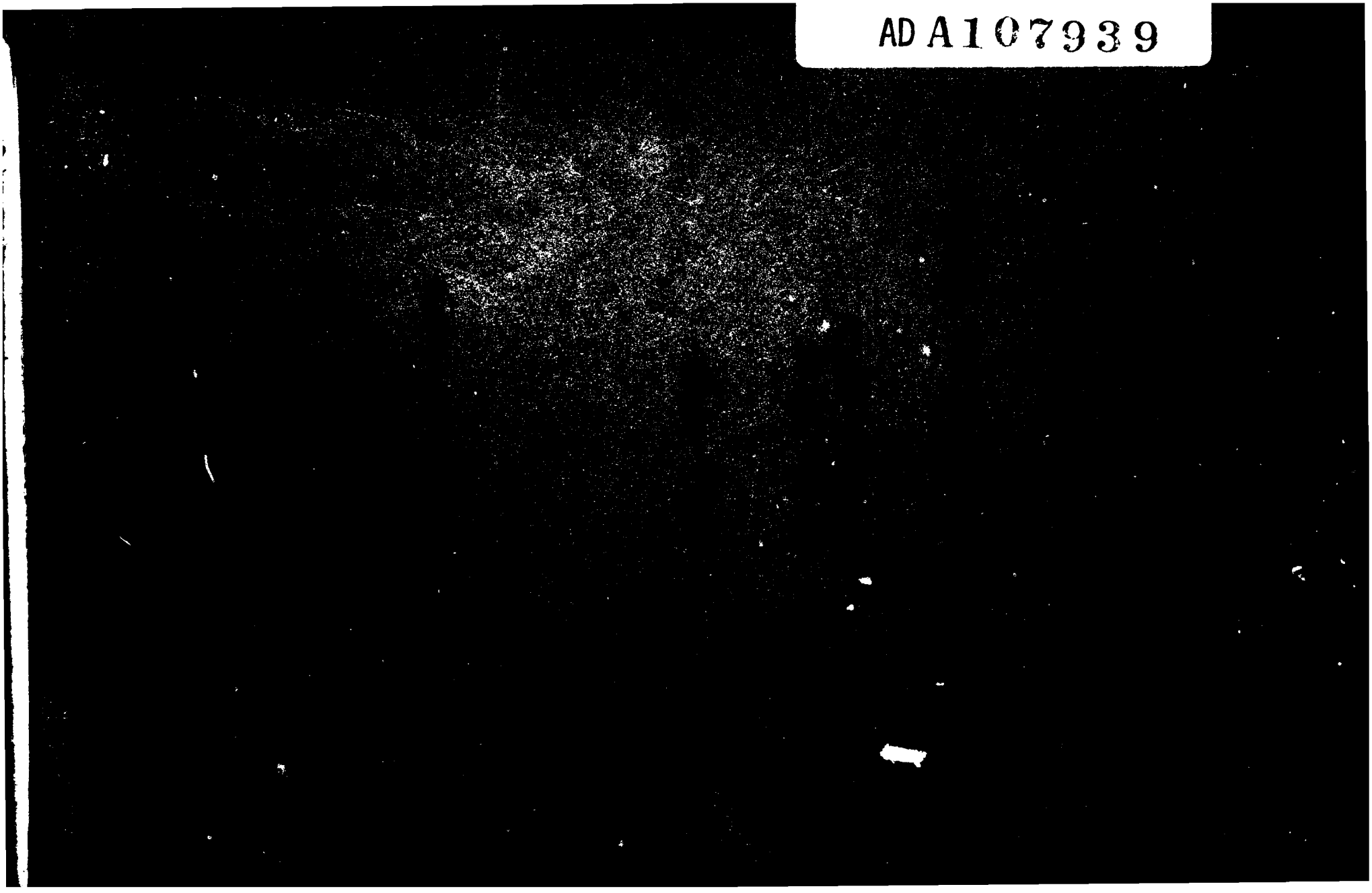

UNCLASSIFIED
SECURITY CLASSIFICATION OF THIS PAGE (When Data Entered)

R&D 2543-EE

REPORT DOCUMENTATION PAGE	READ INSTRUCTIONS BEFORE COMPLETING FORM
1. REPORT NUMBER / 2. GOVT ACCESSION NO. AD-A107939	3. RECIPIENT'S CATALOG NUMBER
4. TITLE (and Subtitle) Submillimetre Laser and Fabry-Perot Spectroscopy using Metallic Mesh	5. TYPE OF REPORT & PERIOD COVERED Final Technical Report June 1978 - June 1981
	6. PERFORMING ORG. REPORT NUMBER
7. AUTHOR(s) Dr. C.R. Pidgeon Dr. B.W. Davis	8. CONTRACT OR GRANT NUMBER(s) DA-ERO-78-G-074
9. PERFORMING ORGANIZATION NAME AND ADDRESS Heriot-Watt University Riccarton, Edinburgh, UK.	10. PROGRAM ELEMENT, PROJECT, TASK AREA & WORK UNIT NUMBERS 6.11.02A 1T161102BH57-03
11. CONTROLLING OFFICE NAME AND ADDRESS USARDSG-UK Box 65, FPO NY 09510	12. REPORT DATE May 1981
	13. NUMBER OF PAGES 39
14. MONITORING AGENCY NAME & ADDRESS (if different from Controlling Office)	15. SECURITY CLASS. (of this report) Unclassified
	15a. DECLASSIFICATION/DOWNGRADING SCHEDULE

16. DISTRIBUTION STATEMENT (of this Report)

Approved for Public Release; distribution unlimited

17. DISTRIBUTION STATEMENT (of the abstract entered in Block 20, if different from Report)

18. SUPPLEMENTARY NOTES

19. KEY WORDS (Continue on reverse side if necessary and identify by block number)

Submillimetre Lasers, CO_2 Lasers, Isotopic CO_2 Lasers, Heterodyne Techniques, CO_2 Mode Properties and Stability, Submillimetre Laser Spectroscopy, Metallic Mesh Spectroscopy, Fine Tuning Characteristics in Submillimetre Lasers, Doppler Splitting, Two

20. ABSTRACT (Continue on reverse side if necessary and identify by block number)

An optically pumped submillimetre laser has been constructed and investigated. Optical pumping with $^{12}C^{16}O_2$ and isotopic $^{13}C^{16}O_2$ has been demonstrated. Using the isotopic $^{13}CO_2$ laser 17 new submillimetre emissions have been reported between 78.5 μm and 917 μm.

DD FORM 1 JAN 73 1473 EDITION OF 1 NOV 65 IS OBSOLETE

UNCLASSIFIED
SECURITY CLASSIFICATION OF THIS PAGE (When Data Entered)

The mode properties, stability and tuning characteristics of the CO_2 laser have been discussed. Such measurements were taken with heterodyne techniques. Cooling effects on the isotopic $^{13}CO_2$ laser have been described and have resulted in increases in both the number of observed lines and output power from the laser.

A high power cw CO_2 laser has also been described and used in the search for new submillimetre emissions.

The submillimetre waveguide laser designed has been shown to give powers in excess of 1 mW throughout the submillimetre region. The design was flexible to permit a choice of coupling and waveguides of various sizes.

The fine tuning characteristics of the submillimetre laser have been investigated. By examination of the Doppler split gain peaks with CO_2 pump offset we have observed Dispersion and Two-Photon Light Shift effects for the first time in cw submillimetre lasers.

Metallic Mesh techniques for the submillimetre region have been investigated. "Inductive" and "Capacitive" type meshes have been characterised. A blocking filter has been produced to suppress the 118.6 μm line in CH_3OH to allow easier identification of larger wavelength lines resulting from the same pumping transition. The successful low temperature performance (< 4 K) of a Low Pass Filter has been demonstrated.

A range of materials suitable for use in the submillimetre region have been characterised.

19. KEYWORDS Cont

Photon Light Shift, Dispersion, new submillimetre emissions, submillimetre filtering techniques, Low Temperature Filters, Materials.

ABSTRACT

An optically pumped submillimetre laser has been constructed and investigated. Optical pumping with $^{12}C^{16}O_2$ and isotopic $^{13}C^{16}O_2$ has been demonstrated. Using the isotopic $^{13}CO_2$ laser 17 new submillimetre emissions have been reported between 78.5 μm and 917 μm.

The mode properties, stability and tuning characteristics of the CO_2 laser have been discussed. Such measurements were taken with heterodyne techniques. Cooling effects on the isotopic $^{13}CO_2$ laser have been described and have resulted in increases in both the number of observed lines and output power from the laser.

A high power cw CO_2 laser has also been described and used in the search for new submillimetre emissions.

The submillimetre waveguide laser designed has been shown to give powers in excess of 1 mW throughout the submillimetre region. The design was flexible to permit a choice of coupling and waveguides of various sizes.

The fine tuning characteristics of the submillimetre laser have been investigated. By examination of the Doppler split gain peaks with CO_2 pump offset we have observed Dispersion and Two-Photon Light Shift effects for the first time in cw submillimetre lasers.

Metallic Mesh techniques for the submillimetre region have been investigated. "Inductive" and "Capacitive" type meshes have been characterised. A blocking filter has been produced to suppress the 118.8 μm line in CH_3OH to allow easier identification of larger wavelength lines resulting from the same pumping transition. The successful low temperature performance (< 4 K) of a Low Pass Filter has been demonstrated.

A range of materials suitable for use in the submillimetre region have been characterised.

KEYWORDS: Submillimetre Lasers, CO_2 Lasers, Isotopic CO_2 Lasers, Heterodyne Techniques, CO_2 Mode Properties and Stability, Submillimetre Laser Spectroscopy, Metallic Mesh Spectroscopy, Fine Tuning Characteristics in Submillimetre Lasers, Doppler Splitting, Two Photon Light Shift, Dispersion, new submillimetre emissions, submillimetre filtering techniques, Low Temperature Filters, Materials.

TABLE OF CONTENTS

Page

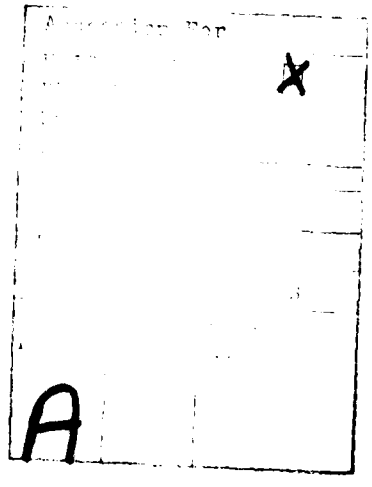

FIGURE CAPTIONS

CHAPTER I

1.1 Partial Energy diagram of N_2 and CO_2 showing laser transitions at 9.3 μm and 10.6 μm.

1.2 Detailed laser transition diagram for the $00^0 1 - 10^0 0$ band (including rotational levels).

1.3 Observed frequency ranges of isotopic CO_2 laser bands.

1.4 Experimental arrangement of the CO_2 heterodyning system.

CHAPTER II

2.1 Schematic partial energy diagram of a polar molecule.

2.2 The mirror translation system

2.3 Schematic diagram of laser

CHAPTER III

3.1 Variation of submillimetre output power (λ = 152.9μm) in EH_{11} mode as resonator length is varied (ΔL). Lower scale shows submillimetre frequency scale deduced from the Fabry-Perot relationship $^{13}CO_2$ 10R(18) laser offset frequency 22.7 $\pm$ 0.5 MHz.

3.2 Observed splitting of $^{15}NH_3$ (λ = 152.9 μm) submillimetre gain maximum $|2\Delta_2|$ as a function of $^{13}CO_2$ 10R(18) pump frequency offset; the pump power and submillimetre laser pressure were set just below the values required for the onset of Autler-Townes splitting. Circles show the experimental data, and the solid line the slope expected from rate equation theory.

3.3 Observed variation of $|2\Delta_2|$ with Δ for CH_3OH (λ = 118.8 μm) pumped by $^{12}CO_2$ 9P(36) under the same conditions as Fig. 3.2

3.4 $^{15}NH_3$ (λ = 152.9 μm) laser EH_{11} mode output power variation (arbitrary units) as resonator length is varied for $^{13}CO_2$ 10R(18) laser input power levels of 0.05 W (A), 0.08 W (B) and 2.3 W (C). Lower scale shows submillimetre frequency scale deduced from the Fabry-Perot relationship.

3.5 Submillimetre heterodyne system for direct frequency determination.

CHAPTER IV

APPENDIX 1

LIST OF TABLES

CHAPTER I

cw CO_2 LASERS

1.1 INTRODUCTION

cw CO_2 lasers are used as driving sources for the submillimetre laser described within this report.

The PL_3 cw CO_2 laser intended for use as a pump laser in the testing of the submillimetre laser has been extensively investigated and the method by which the characteristics of the CO_2 laser were obtained is described. A higher power CO_2 laser, the PL_4, is also described later within this chapter. The effect of isotopic substitution in CO_2 gas mixes is also described.

Although the absorption lines of vibrational-rotational molecular transitions commonly used as driving transitions in optically pumped submillimetre lasers are typically Doppler broadened to $\sim$ 50 MHz full width half maximum (F.W.H.M.), the operating pressures of cw lasers are normally restricted to pressures well below 1 torr, where pressure broadening is only $\sim$ 1 MHz. The narrow radiation linewidth produced by a cw CO_2 laser therefore selectively excites only a small fraction of the available molecules, those with Doppler-shifted absorption frequencies lying within the homogeneous linewidth of the actual CO_2 laser frequency. Tuning of the CO_2 laser, by means of a piezo-ceramic attached to the output coupler, over its pressure broadened gain linewidth of $\sim$ 3.5 MHz/torr will therefore selectively excite different groups of molecules lying under the Doppler envelope, resulting in a corresponding tuning of the peak of the submillimetre gain. Since the finesse of typical submillimetre resonators is high, changes in the CO_2 laser frequency due to thermal shifts, mechanical instabilities or mode changes are accordingly strongly reflected in the submillimetre output power level. The consequence of this is that the CO_2 laser should have well controlled and stable frequency tuning characteristics if a stable submillimetre laser output is to be achieved.

1.2 GENERAL PRINCIPLE OF OPERATION

The N_2-CO_2 laser operation has been shown to arise from the selective excitation of molecules through the vibrational energy transfer from a diatomic molecule [1] .

While laser action can occur between the vibrational levels of CO_2 alone, the provision of additives can enhance laser action [1] . Additives are utilized in the gas mixes used in the work described and are discussed later in this section..

The partial energy diagram for the N_2-CO_2 transition is shown in Fig 1.1, with a more detailed laser transition diagram for the 10.6 μm, 00^01 - 10^00 transition given in Fig 1.2.

The effect of N_2 is seen in Fig 1.1 and the remaining additives used are now described. In a flowing gas mix the only addition to the N_2-CO_2 combination would be Helium. The role of Helium is two fold; to aid the depletion of the 01'0 level by reducing its lifetime [2] and so reducing any bottleneck effect and secondly the gas helps in keeping the CO_2 cool by conducting heat to the walls of the discharge tube by virtue of its high thermal conductivity.

In a sealed off situation additional additives are required. Hydrogen (H_2) is added to reduce the oxygen which is generated in the dissociation of CO_2:

$$CO_2 + e \rightarrow CO + e + O$$
$$H_2 + O \rightarrow H_2O$$
$$H_2O \rightarrow OH + O$$
$$OH + CO \rightarrow CO_2 + H_2$$

which restores the CO_2 concentration.

The addition of Xenon, which increases the number of electrons available for collisions, helps reduce the discharge temperature since a lower discharge current can be used. With the additives described, the percentage combination of gases will now be described for the various lasers (each laser requiring an optimized combination). Table 1.1 gives details of the gas combinations.

1.3 THE PL_3 CO_2 LASER

The cw PL_3 CO_2 laser investigated is of conventional design, comprising of a sealed water cooled 10 mm ID discharge tube with an internal 10 m concave semitransparent (30%) output coupler and an adjustable blazed diffraction grating. The 1.78 m optical resonator is supported by a strong structure of granite and four 1" thick invar bars, giving good mechanical and thermal stability [3]. The laser could be operated in a 'sealed' or 'flowing' gas mode, but the results presented are for sealed operation. Flowing gas operation, although resulting in higher output powers, does have a detrimental effect on the frequency stability of the laser. The different gas mixes have been described in section 1.2. c.w. output power levels of 15 W at band centre are easily available using the sealed off gas mix (with $\sim$ 25 W flowing).

1.4 ISOTOPICALLY ENRICHED CO_2 GAS MIX

1.4.1 The Isotopic Gas.

The isotopic substitution in molecules has been shown to result in changes in the molecular spectra of the molecule [4], and so giving the possibility of new CO_2 laser transitions. The use of

this technique in CO_2 has resulted in $\sim$ 400 new lasing wavelengths in the 9-12 μm region [5,6]. The new IR pump lines have been derived from $^{12}C^{18}O_2$, $^{13}C^{16}O_2$, $^{13}C^{18}O_2$ and $^{14}C^{16}O_2$ as shown in Fig 1.3.

The isotopic CO_2 laser is operated "sealed off" due to the high cost of the mix. With the PL_3 a sealed off lifetime of 1-2 months was possible. This extended operation was due to the ultra-high vacuum components used in the PL_3 construction. The mix used was as described in table 1.1 for the PL_3 sealed, but with $^{13}C^{16}O_2$ (90% atomic)replacing the $^{12}C^{16}O_2$.

Cooling of the gas mix has been found to improve power output and also increase the number of lasing lines and this is described.

1.4.2 Cooling Effects

The effect of varying the temperature of the cooling supply used with the isotopic gas mix has been investigated. It has been shown that increased performance is achieved by cooling of the supply down to $\sim$ -60°C [5] but in the work carried out the optimum was found to be at 0°C. The laser was cooled with a continuous flow of ethylene glycol at a temperature of -15°C and the output power from the laser monitored as the temperature was allowed to rise. The change in output power was $\sim$ 0.1 W/°C with the optimum found at 0°C. The power observed was 3.5 Watts at 0°C, but this power was later increased by suitable adjustments to pressure and discharge current. Another apparent advantage of cooling the isotope mix was seen in the increase in the number of laser lines present. At room temperature very few emission lines were observed ($\sim$ 9 total).

The relative ease of operation in sealed conditions, linked with the long lifetime of one fill of gas could make the isotopic CO_2 laser an extremely useful source of I.R. frequencies. The realization of the application of this type of laser in optical pumping has been shown. A programme was set up to investigate the possibilities of any frequency coincidences between the I.R. frequencies and the absorption lines in polar molecular species and the results of this application are described in Chapter 2.

1.5 HETERODYNE TECHNIQUES USED TO DETERMINE CHARACTERISTICS OF THE PUMP CO_2 LASER

1.5.1 The Optogalvanic Effect and Heterodyne Techniques.

To determine the frequency stability and tuning characteristics of the PL_3 CO_2 laser, a heterodyning technique was used. This is a simple technique which uses two near coincident frequencies from different sources to give sum and difference beat frequencies, from which information about one of the sources can be derived. To enable measurements of any meaning to be made, however, one of the sources must be fixed in frequency. Any instabilities in the

other source may then be observed, relative to the fixed laser source.

The method was to mix the laser outputs from the two CO_2 lasers one of which was optogalvanically stabilized [7]. The optogalvanically stabilized laser was of similar design to the main laser, but with a 1 metre cavity and with passive stability provided by three 1" diameter invar bars. Active stabilization was provided by the method now described.

An electronic feedback loop system was used to control the laser cavity length. The cavity length was modulated through the piezoceramic which was attached to the output coupler. The effect of the cavity length modulation is to give a modulation of the internal field intensity [7] and any changes in this intensity are seen in the discharge impedance which can then be seen as a current fluctuation (the optogalvanic effect). A d.c. correction voltage is then applied to the piezoceramic to maintain oscillation at line centre. By this method the reference laser could be locked to $\sim \pm$ 0.2 MHz of the natural line centre of the lasing transition.

For frequency measurements, a small fraction of the main CO_2 beam is split off with a NaCl beam splitter and mixed with the beam from the optogalvanically locked CO_2 reference laser. This is shown in Fig 1.4.

The mixed outputs were then incident onto a PbSnTe liquid nitrogen cooled detector and the resultant beat note generated then displayed on a spectrum analyzer, immediately indicating the frequency components present in the main CO_2 laser beam. By observation of the displayed signal it was possible to determine the stability and tuning range of the CO_2 laser.

1.5.2 Mode Structure and Tuning Characteristics of the CO_2 Laser

In describing the results of the measurements made, it is convenient to distinguish between CO_2 laser lines at the band centres and on the band wings. The lines lying close to the band wings, where the laser gain is lower, were observed to always produce a single beat note on the spectrum analyzer, tunable piezoelectrically by up to $\sim$ 35 MHz about the natural CO_2 line centre. The corresponding far field mode pattern was always circularly symmetric and uniform, indicating that the mode observed was the TEM_{oo} mode. Burn patterns, on heat sensitive paper, close to the laser output were generally complex, and not of a Gaussian appearance; this is attributed to rapidly divergent rays of the same frequency as the TEM_{oog} mode, perhaps caused by internal scattering or wall reflections within the discharge tube.

Laser lines lying near the centre of the CO_2 bands were generally found to contain three distinct frequency components: a single frequency, together with two other closely spaced frequencies (about 0.5 MHz apart) lying about 17 MHz higher in frequency. All frequencies tuned at the same rate as the piezo-electric drive were varied, maintaining their relative separations. It was found to be a simple practical matter to reduce the laser discharge current steadily until either the "single" frequency or the "double" frequency ceased to oscillate so that essentially single frequency oscillation was obtained (i.e. that of the component lying closest to the gain centre). In this manner it was possible to operate the laser with the "single" frequency oscillating alone at frequencies lower than the natural CO_2 line centre, and with the "doublet" completely alone over all frequencies higher than the natural CO_2 line centre. Using these two regimes of operation, it was found that the single frequency was characterised by a Gaussian-like far field burn pattern, whilst the "doublet" was characterised by a more complex pattern (commonly an annulus) critically dependent upon fine adjustment of the diffraction grating.

Inspection of the standard expression for the mode frequencies of an open resonator shows that the Gaussian TEM_{oo} mode should always be the lowest frequency present, in agreement with the above observation. The "doublet" mode lying 17 MHz higher in frequency is most probably the almost degenerate TEM_{01} and TEM_{10} modes.

1.5.3 Stability Measurements

The short term instability of the output frequency was better than 100 kHz over a 1 sec period and was less than the jitter modulation of the reference heterodyne laser ($\pm$ 0.7 MHz). The rigid mechanical construction of the laser enabled moderate shocks near the laser to perturb the laser frequency by less than 1 MHz, and under normal laboratory room conditions the thermal stability of the structure was sufficient to produce thermal drifts of less than 1.6 MHz over a ten minute period.

The measurements presented have confirmed that the cw CO_2 laser will be suitable for optically pumping a submillimetre laser.

Work is in progress to observe the effect of CO_2 pump quality on the submillimetre laser output and this will be reported at a later date.

1.6 THE PL_4 PUMP LASER

In addition to the PL_3 laser described there developed a need for a higher power CO_2 laser. The EI PL_4 was such a laser with a single arm discharge and of simpler design that the PL_3. The PL_4 [8] was grating tuned with a piezo fine tuning facility attached to the output coupler. Both grating and output coupler were

external to the discharge tube, which had two ZnSe Brewster windows forming the vacuum seal at either end. The laser cavity which was invar stabilized, was 1.8 m long with a discharge length of 1.3 m. This laser was capable of giving up to 75 W cw with a flowing $^{12}C^{16}O_2$ gas mix.

The lifetime of a sealed off gas mix was not as long as with the PL_4, with the main reason being due to the 'O' ring seals in the PL_4 .

This laser was used in an experiment to produce new sub-millimetre lines from isotopic $^{13}CO_2$ pumping.

CHAPTER II

AN OPTICALLY PUMPED SUBMILLIMETRE LASER.

2.1 INTRODUCTION AND BASIC THEORY

The optically pumped submillimetre laser was first described in 1970 [9] and is now a commonly used source of coherent submillimetre radiation. The accidental coincidences between Infrared frequencies and Doppler broadened vibrational-rotational absorption lines of polar molecules have given rise to over 1000 submillimetre wavelengths ranging from tens to thousands of microns [10].

The optically pumped laser system required for the generation of submillimetre emission consists of an I.R. pump (typically CO_2) and a submillimetre laser. The CO_2 laser should be frequency tunable over as wide a range as possible and be stable in frequency. The excitation of a particular rotational level within some vibrational level with an I.R. frequency is a selective process giving the opportunity of an efficient laser system. The quantum efficiency can be as high as 30% [10], but such high efficiencies were not achieved until the advent of the waveguide type laser [11], with the original optically pumped submillimetre laser, being of the open resonator type and only yielding quantum efficiencies of a few percent or less.

Lasing action occurs between adjacent rotational levels within some vibrational state providing certain conditions are met.

A schematic partial energy diagram for a polar molecule is shown in Fig 2.1, and the following description uses terms shown in the figure.

One such condition is that the molecule should be polar, and that the permanent dipole moment μ should be $\simeq$ 1 Debye or larger, since the transition probability is directly proportional to the permanent dipole moment. The close coincidence between the I.R. source and absorption line is typically less than $\sim 0.01\ cm^{-1}$ (50 MHz), although this can be relaxed with high pump powers.

The pressure of the gas used in submillimetre optical pumping has been found to be within the range, 30 mT - 300 mT and such low operating pressures result in the vibrational-rotational absorption lines being broadened by a Doppler type process. Such pressures are required to avoid rapid thermalization of the rotational levels, a process which is proportional to pressure, and is given by collisions occurring at a rate $\tau_{\Delta J}^{-1}$ (λ) and occurs in all vibrational levels.

Another molecular relaxation rate Γ, shows the rate at which molecules in some upper vibrational states, relax to a ground state. This rate has been shown, at the pressures used to be largely due to collisions with the resonator walls, which is dependent on the molecular diffusion rate across the resonator.

The relative values of λ and Γ are critical for a population inversion to be sustained, and Γ must be sufficiently rapid to avoid a build up of population in the lower laser level, which in turn would result in the destruction of inversion. The cavity design has been shown to effect the vibrational relaxation rate Γ, with the waveguide type cavity greatly enhancing Γ.

The laser was thus constructed as a waveguide type but with the possibility of modifying to an open resonator type at a later stage.

A number of aspects relating to the submillimetre laser have been investigated and are discussed. Although over 1000 submillimetre emissions have been seen the use of such lasers will not be fully utilized until a more complete frequency coverage of the submillimetre range is achieved. The application of isotopic CO_2 pumping is one method by which this aim can be reached.

The technique was first shown in our laboratories with $^{15}NH_3$ being pumped by the 10R18 transition in $^{13}CO_2$ [12] and the extension of the technique is described in Section 2.4, where 17 new cw submillimetre emissions are reported [13].

The tuning characteristics of the submillimetre laser have been investigated and such work has revealed a nonlinear relationship between the Doppler-Split gain peaks and the CO_2 pump frequency. Such effects are described in terms of dispersion and the two photon light shift [14,15], and are presented in Chapter III.

2.2 THE SUBMILLIMETRE LASER DESIGN

A laser which could easily accommodate a wide range of waveguides and output coupling systems, but still retain performance with submillimetre powers in excess of 1 mW over the whole submillimetre range, was required and the following is a description of the laser so designed [16].

From previous work with an EI 195 waveguide type, it was found that the reflectors at the input and output ends of the laser could easily be aligned parallel with an external HeNe laser beam. This relaxed the design task since no serious problems would be experienced in translating one of the reflectors against a pressure difference (atmospheric outside the cavity and typically 10^{-1} torr inside) if both reflectors were inside the vacuum. Other designs have been seen to use a set of flexible bellows loosely connected to the output coupler, with the bellows providing the required spring effect for a smooth translating motion for the output coupler, but this can be extremely costly and for this reason an alternative was investigated in the form of a 'wobble stick', and is described later.

The main criteria for the laser can be given as:

(1) Simple construction.
(2) Flexibility in waveguide and reflector choice.
(3) Output coupling method to be such that all known systems of coupling could be introduced.
(4) Sealed or flowing gas operation.

The condition that the output coupling method should be flexible led to the input mirror being the one which was translated (this being necessary to tune the cavity) and the output mirror being 'fixed'. The problem, however, of a focussed CO_2 beam being on axis with the submillimetre laser, suggested that if a direct on axis mirror drive system was used then there would be a possibility of danger to the operator unless a remote drive system was incorporated. The alternative was to use a 'wobble stick' with side entry into the laser as shown in Fig. (2.2). This arrangement has the useful characteristic that a movement of say x μm appears as a movement of the translator of $\sim x/3$ depending on the ratio of the distances XA to XB. Stainless steel bellows (1) were used to give a spring motion. A roller ball bearing (2) ensured that frictional forces between the micrometer drive and the swinging arm (3) were kept to a minimum. The other end of the swinging arm made contact with a translator, onto which the input mirror was fixed, with a second roller ball bearing (4). A pushing motion is experienced by the translator for a pulling motion by the rotating flange (5), attached to the micrometer. The motion of the translator was over two tracks constructed out of ball bearings laid in tracks defined by stainless steel bars.

Vacuum integrity of the laser was maintained with standard muff coupling type 'O' ring seals at all joints. This has been effective, in that the ultimate vacuum attainable with a diffusion pump is $\sim 10^{-5}$ torr. No degradation of the 'O' rings, which are all Viton has been observed over the period of operation.

The design of the resonator is outlined in Fig. (2.3), with the whole laser being mounted on a rigid aluminium channel (A). At each end of the channel, two aluminium blocks (B) and (C) were fixed securely onto support brackets (E). One of the brackets is rigidly fixed to the base with the other being free to slide along the laser axis. This freedom of motion was necessary to free the structure from any distortions resulting from any thermal effects. The amount of thermal motion is kept to a minimum with the use of three invar bar supports (D) to separate the end blocks. The low coefficient of expansion of invar makes it a suitable material. Additional support for the 1.5 metre bars was provided by support flanges at (1) and (2).

The aluminium blocks (B) and (C) were bored out to give cavities in which the output and input reflectors could be housed. The input mirror, as discussed, was translatable by ~ 5 mm, and this was in block (C). The output mirror support was rigidly fixed internally to block (B). Both mirrors could be easily adjusted with the laser cavity unevacuated.

An outer vacuum jacket was provided by means of a glass tube, 84 mm diameter, and was fixed by muff type coupling seals to the two end blocks. The size of the outer vacuum envelope, linked with the large coupling mirrors (50 mm diameter) enables waveguides of up to ∿ 48 mm I/D to be used in the system. Alternatively an open resonator laser could easily be produced from such a design. The pump powers required for efficient pumping of large bore waveguides were in excess to those available with our cw CO_2 lasers.

Vacuum pumping was from a port in block (C) using a diffusion pump, although this was later changed to an ion pump system. The change was necessitated because of the instabilities caused by the backing rotary pump. Operation with the ion pump system had no such problems and the results presented are for such a system. The laser gas inlet is through a port in block (B), at the opposite end of the laser. Provision for an internally mounted optoacoustic facility is provided with a vacuum lead through positioned below the gas inlet.

The optoacoustic effect is commonly used to determine absorption in gases [17] and has been used to great effect with submillimetre lasers. A small microphone was inserted in the vacuum space, close to the output coupler, with electrical lead throughs for power supply and signal output. Absorptions in the gas are seen as pressure changes which in turn are sensed by the microphone. Such a system was utilized in the search for new submillimetre lines with isotopic $^{13}CO_2$ pumping (Section 2.4).

The final vacuum seals in the laser are provided by flat end flanges which are clamped onto the end blocks with 'O' ring seals. These flanges support the input and output windows, NaCl and T.P.X. respectively.

At a later stage the NaCl was substituted by a ZnSe input window. The relatively short lifetime of NaCl was the reason for the change. The output window was of a large enough diameter so as not to impede any of the diverging radiation emerging from the hole coupler.

The input mirror had a centrally drilled hole of 2 mm diameter, through which the CO_2 radiation was injected, although this diameter is not too critical.

It was important however to ensure that the diameter was larger than the focussed CO_2 spot size.

The output hole was 5 mm diameter, again centrally drilled. A 25 mm I/D dielectric waveguide (F) was held coaxially inside the outer glass envelope (G). The waveguides are 1.5 metres long resulting in a minimum cavity length of the same and a maximum cavity length of ∿ 1.505 metres.

With the system of end blocks giving housing for the reflectors it will be a relatively simple task to remove one completely and install a Michelson type mesh coupler if required. Such an arrangement would be supported by the end flange (E) in a similar fashion to that of the original design.

2.3 LASER OPERATION AND MODIFICATIONS

The main changes to the original design were to the translator mechanism. The stainless steel bellows were a replacement for brass bellows which began to work harden after 1-2 months of operation. The swing arm was also noticeably flexing and was subsequently replaced by a larger diameter bar.

This modification had a working lifetime of 12 months after which the stainless bellows began to work harden. The original design of having a side entry system for the translator has now been changed to accommodate a straight through translator. A new end plate has been designed to permit a micrometer to be mounted with an 'O' ring vacuum seal.

For a period of time the laser was operated with a modification to the vacuum jacket system. The outer jacket was discarded and the waveguide itself was arranged to complete the vacuum.

Using the CO_2 laser described in the first Chapter, a series of tests on the submillimetre laser were carried out and the results of the laser performance, for a range of laser gases, are shown in table (2.1).

The original objective of laser power in excess of 1 mW over the whole submillimetre range has been achieved. For wavelengths greater than 500 μm, brass wave guides were used (the losses in dielectric guides being excessive for $\lambda \geq 500$ μm). The brass guide dimensions were as for the original dielectric guide.

2.4 NEW SUBMILLIMETRE LINES PRODUCED FROM A SUBMILLIMETRE LASER WITH ISOTOPIC $^{13}C^{16}O_2$ PUMPING.

2.4.1 Introduction

Earlier in this Chapter the first application of the isotopic $^{13}CO_2$ laser to the optical pumping of submillimetre lasers was described with the 10R18 transition in $^{13}C^{16}O_2$ pumping $^{15}NH_3$ to produce a new submillimetre emission at 153 μm [12]. Such a technique suggested the possibility of extending the coverage in the submillimetre region by virtue of the fact that an increase in the number of possible coincidences between I.R. frequencies and submillimetre absorptions should result from the extra I.R. frequencies produced from isotopic substitution. The isotopic CO_2 laser has been described in Chapter 1.

An optoacoustic survey of a number of known lasing media with $^{12}C^{16}O_2$ pumping was performed using the PL_3 laser with a sealed off mix of $^{13}C^{16}O_2$, and by further using a PL_4 pump laser, 17 new submillimetre laser emissions over a large range were discovered.

2.4.2 Experimental Results

Using the PL_3 to perform the optoacoustic search of molecules a recording of all the absorptions was made. Each absorption was investigated, making appropriate adjustments to submillimetre cavity length, gas pressure and CO_2 frequency offset, with the intention of finding submillimetre laser emission. No lasing action was observed with the system described and this was attributed to the low pump powers from the PL_3 laser ($\sim$ 12 W at band centre).

The PL_4 laser, as described in Chapter I was used as an alternative to the PL_3 because of its capability to produce higher output powers. Using the same isotopic gas mix up to 20 W cw could be obtained at band centre. The $^{13}C^{16}O_2$ radiation from the PL_4 was focussed with a 50 cm concave mirror into the submillimetre waveguide cavity, through a 1 mm pinhole. As before, the submillimetre radiation was extracted through a 5 mm hole coupler and a 6 mm T.P.X. vacuum window. A 24 mm diameter 1.5 m long brass waveguide was used to ensure low waveguide losses in the long wavelength region [18,19].

The molecules investigated are shown in Table 2.2. The waveguide cavity was normally evacuated to $\sim 10^{-4}$ torr with a two stage rotary and ion pump rig. The molecule under test was then released into the cavity and investigated. When the molecules used were in liquid form an additional process was required before releasing into the cavity. De-airing of the liquid has been found to reduce the power threshold for lasing action, yet little effect has been noticed in final output power. The process is achieved by the freeze-pump-thaw method, with two or three cycles normally being sufficient to remove air contaminents from the liquid chemical. Adjustments to laser operating conditions were repeated as described and a number of lasing transitions were identified.

A total of 17 new submillimetre emissions have been observed and these are given in Table 2.3. The spread of wavelengths, 78.5 μm to 917 μm indicates the suitability of the isotopic CO_2 laser for the generation of new emissions, and further suggests the possibility of using other isotopes of CO_2 to generate more emissions.

The wavelengths were measured by the use of external mesh Fabry-Perot interferometers. Three sets of meshes were chosen for optimum performance over the range of wavelengths discussed and have been characterised in Chapter IV. The interferometers

were placed immediately in front of the detectors used and an accuracy of ± 0.3 μm could be achieved. This figure was a result of scanning over as large a number of orders as possible. This number was only limited by the available micrometer travel on the interferometer. The ultimate accuracy at 917 μm (± 3 μm) was thus limited by the fact we could only scan a few orders.

The submillimetre power was measured with pyroelectric and Golay detectors which had been previously calibrated against a Laser Instrumention thermopile (14BT) [20].

The two emissions (A) associated with NH_3 (natural abundance) were only observed when small traces of CD_3OD were present in the laser cavity. Initial investigations have been performed using other molecules mixed with NH_3. A known buffer gas, n-hexane [21] and CH_3OH were added separately to NH_3 in a similar fashion as with CD_3OD but no lasing action resulted. No lasing was observed for small amounts of NH_3 in a bulk of CD_3OD. It was further noted that the $^{13}C^{16}O_2$ 10P24 transition pumping $^{15}NH_3$ yields a different wavelength when pumping the NH_3/CD_3OD mixture , whereas the $^{13}C^{16}O_2$ 10P14 transition pumping both $^{15}NH_3$ and NH_3/CD_3OD yields identical FIR emissions. An optimum concentration of CD_3OD has been observed with FIR output powers, cut-on and cut-off points being dependent on the relative concentrations of the two molecules. The explanation for the described result is not fully resolved and further work to determine the process which was taking place is required.

We have further observed lasing action at 152.9 μm in NH_3 (B) which had previously been observed in $^{15}NH_3$ [12]. The operating pressure of this line was 400mT and is consistent with the low concentration of ^{15}N in ammonia of natural isotopic abundance.

CD_3OD has been shown to be a useful molecule with 5 consecutive $^{13}C^{16}O_2$ pump lines (9P12 to 9P20) yielding 5 different FIR emissions ranging from 167.5 μm to 533 μm.

We have also observed two new submillimetre emissions in CD_3OD pumped with the normal $^{12}C^{16}O_2$ laser. Table 2.4 lists the relevant details.

Examination of the powers recorded indicate that most of the observed wavelengths have powers in excess of 1 mW, which is consistent with our original objective. Further work in this field is planned with the use of other submillimetre gas media and other isotopes of CO_2.

CHAPTER III

FINE TUNING CHARACTERISTICS OF OPTICALLY PUMPED SUBMILLIMETRE LASERS

3.1 INTRODUCTION

To understand further the operation of the submillimetre laser the tuning characteristics of the laser were investigated. Detailed measurements of the dependence of the submillimetre output power level emitted by a $^{15}NH_3$ cw optically pumped waveguide laser [12,22,23] on $^{13}CO_2$ input power level, $^{13}CO_2$ laser frequency and submillimetre resonator length changes have been made.

The results have shown that there is a significant deviation between experimental results and rate equation theory as the $^{13}CO_2$ pump frequency approaches the natural ν_2 as Q(5,4) frequency in $^{15}NH_3$. Similar effects have been observed with the 118.8 μm transition in CH_3OH. The deviation has been explained in terms of dispersion and the two photon light shift. Other effects have been observed and these are to be described.

Experimental and theoretical discussions are given.

There has recently been considerable interest in light-induced frequency shifts of atomic and molecular states [24-26], first observed in the near infrared by Toschek and co-workers [25].

Light shifts occur when the atomic or molecular oscillators interact with off-resonant light fields; the effect is related to the Autler-Townes splitting which has been studied extensively in the optical range [27]. Since these effects can give rise to limitations in the determination of atomic and molecular frequencies, their understanding is also of practical importance. This situation applies to the optically pumped far infrared laser (OPFIRL), where anisotropic (two-photon) amplification can occur for a Doppler broadened quantum mechanical three level system interacting with two opposite intense pump laser beams [28,29]. Forward-backward gain anisotropy has been observed [28,30], and the Autler-Townes splitting for co-propagating beams demonstrated in an external gain cell [31]. Such factors are expected to be a major constraint in the use of OPFIRLS for frequency synthesis and high resolution spectroscopic applications [32].

3.2 EXPERIMENTAL DESCRIPTION

The PL_3 pump laser was operated with cw power levels of $\sim$ 10 W on the 10R18 transition of $^{13}CO_2$. The heterodyne technique described in Chapter 1.5 was used to determine the CO_2 pump frequency. The submillimetre waveguide laser used was similar to that described in Chapter II but was of a commercial design, (Edinburgh Instruments EI 195) and was fitted with a precision motorised micrometer and length sensor enabling the submillimetre

resonator length (L) to be varied linearly in time with sub-micron precision.

The consequence of using the extremely high efficient $^{15}NH_3$ transition was that submillimetre lasing action could be sustained with very low pump powers and submillimetre gas pressures. For the experiments described the laser was filled with $^{15}NH_3$ with typical pressures of 10 to 30 millitorr, with threshold input power levels as low as 10 mW [12].

At operating pressures of less than 50mtorr the absorption of $^{13}CO_2$ radiation in the submillimetre resonator is small, enabling a longitudinal standing wave of $^{13}CO_2$and submillimetre radiation to be set up within the waveguide resonator. This standing wave will excite two velocity groups of $^{15}NH_3$ molecules within the Doppler broadened (82 MHz FWHM) ν_2 as Q(5,4) absorption transition, with velocity components $v_\pm$ along the waveguide axis given by $v_\pm = \pm c\ \Delta_1/\Delta_0$, where Δ_1 is the detuning of the $^{13}CO_2$ laser frequency from the natural absorbing frequency Δ_0 of the ν_2 as Q(5,4) transition. The two velocity groups so excited generate two maxima in the submillimetre gain lineshape, with a homogeneously broadened linewidth of $\sim$ 1 MHz at 20 mtorr pressure, and a Doppler splitting $2\Delta_2 = 2\Delta_1\ \lambda CO_2/\lambda_{sub}$. We have made accurate measurements of this splitting by scanning the submillimetre resonator length whilst recording the induced variation of the output power at 152.9 μm; peaks in the emitted power occur whenever a natural Fabry-Perot submillimetre mode of the waveguide resonator coincides with a gain peak.

The lowest order EH_{11} mode of our waveguide resonator has a propagation loss of less than 1% per metre [18], so that this mode has an end-mirror limited line width of $(c/2L)\ (1 - R)/\pi\sqrt{R}$ $\sim$ 1 MHz, where R is the effective end-mirror reflectivity. Most measurements were made using this mode, since it naturally generated the greatest output power level; a few measurements which were made using higher order resonator modes yielded identical Doppler splitting measurements. Fig 3.1 shows a typical experimental recording of the EH_{11} mode submillimetre output power level at λ = 152.9 μm as the submillimetre resonator length was scanned, using low $^{13}CO_2$ input power and a $^{13}CO_2$ laser frequency 22.7 $\pm$ 0.5 MHz higher than the natural $^{13}CO_2$ 10R(18) laser gain linewidth centre. Maxima in the output power may be determined from such recordings with a resonator length precision of $\pm$ 0.03 μm, corresponding to an uncertainty of $\pm$ 100 kHz in the separation of the two submillimetre gain maxima. Fig 3.2 shows the results of a series of such measurements (open circles) for a wide range of $^{13}CO_2$ 10R(18) laser frequencies, measured with respect to the natural $^{13}CO_2$ 10R(18) laser gain linewidth centre; the natural line centre frequency of the ν_2 as Q(5,4) $^{15}NH_3$ absorption frequency was determined by a subsidiary measurement of the transferred Lamb dip [33] to be -12.4 $\pm$ 1 MHz, shown by the solid circle in fig.3.2. The

Doppler splitting expected by rate equation theory $2\Delta_1 \lambda CO_2/\lambda_{sub}$ is shown by the solid line in fig.3.2,taking the above value for the natural ν_2 as Q(5,4) line centre frequency and taking λ_{sub} = 152.9 μm [12]. A significant deviation between experiment and rate equation theory can be seen to occur as the $^{13}CO_2$ laser frequency approaches the natural ν_2 as Q(5,4) frequency. An identical series of measurements were also made in CH_3OH using the weaker (compared to 152.9 μm) submillimetre lasing transition at 118.8 μm. The results for CH_3OH, shown in Fig 3.3 show a similar but less pronounced anomaly as the 9P(36) $^{12}CO_2$ laser frequency approaches the natural CH_3OH absorption line frequency (23.6 $\pm$ 0.5 MHz, solid circle).

These deviations from the rate equation have been attributed to dispersion and two photon light shift effects and are the first such observations in optically pumped submillimetre lasers, and are discussed in Section 3.3.

At high $^{13}CO_2$ input power levels the experimental recordings become more complex than those shown in fig 3.1. A series of recordings are shown in Fig 3.4 with increasing $^{13}CO_2$ input power, at a fixed CO_2 frequency of 17.7 $\pm$ 0.5 MHz above the natural $^{13}CO_2$ 10R(18) gain linewidth centre frequency. The high frequency submillimetre peak (copropagating molecular velocity group) is seen to broaden and split with increasing $^{13}CO_2$ input power. This is attributed to a dynamic Stark splitting within the laser, an effect previously only reported in external gain cell measurements [34]. The line sharpening of the counterpropagating component is observably due to a sudden "switching off" of the submillimetre emission as a critical resonator length is reached; this switching effect is also visible on the copropagating component in recording (B) of Fig 3.4. This effect is not fully understood, but is very similar to saturable-absorber switching observed in an HCN laser using an intra-cavity saturable absorbing gas [35].

3.3 THEORETICAL ANALYSIS FOR THE TWO PHOTON LIGHT SHIFT EFFECT.

As described, light shifts occur when atomic or molecular systems interact with non-resonant light fields: we are defining a two photon light shift as the shift of a two photon resonance - the submillimetre laser transition - by a third, non resonant field,in this case the second pump component. In order to identify the mechanism(s) for these effects we must examine the submillimetre polarisation in some detail.

In lowest order ($\chi^{(3)}$) the spatially-averaged submillimetre polarisation due to a molecule of longitudinal velocity component v is determined by the Lorentzians:

$$D_{32}(\Delta_2) = (\Delta_2 - k_2 v + i\gamma_{32})^{-1}$$

$$D_{21}(\Delta_1) = (\Delta_1 - k_1 v + i\gamma_{21})^{-1} \qquad (3.1)$$

$$D_{13}(\Delta_1-\Delta_2) = [\Delta_2-\Delta_1 - (k_2-k_1)v + i\gamma_{13}]^{-1}$$

where we adopt the conventions of Feldman and Feld [36], but have relabelled the levels to a more conventional 1-2-3; γ_{21} and γ_{32} are the homogeneous linewidths of pump and FIR transitions respectively. Since both fields are standing-wave in nature, corresponding terms with k_1 and/or k_2 changed in sign also exist. We adopt however the standard "weak-probe" approximation, and need thus consider only $k_2 > 0$. The pump field component E_+ with $k_1 > 0$ (co-propagating) then induces Autler-Townes splitting to order $\chi^{(5)}$ [36], whereas E_- ($k_1 < 0$) gives only a single "fluorescence" peak, as observed.

Even to order $\chi^{(5)}$, the contributions to the FIR gain are many, of which we instance three in symbolic form:

$$\rho_{11}\ \overset{E_+}{\rightarrow}\ \rho_{21}\ \overset{E_2}{\rightarrow}\ \rho_{31}\ \overset{E_+^*}{\rightarrow}\ \rho_{32}\ \overset{E_\pm}{\rightarrow}\ \rho_{31}\ \overset{E_+^*}{\rightarrow}\ \rho_{32} \quad \ldots\ldots \quad (3.2a)$$

$$\rho_{11}\ \overset{E_+}{\rightarrow}\ \rho_{21}\ \overset{E_+^*}{\rightarrow}\ \rho_{22}\ \overset{E_-}{\rightarrow}\ \rho_{21}\ \overset{E_-^*}{\rightarrow}\ \rho_{22}\ \overset{E_2}{\rightarrow}\ \rho_{32} \quad \ldots(3.2b)$$

$$\rho_{11}\ \overset{E_+}{\rightarrow}\ \rho_{21}\ \overset{E_-^*}{\rightarrow}\ \rho_{22}\ \overset{E_-}{\rightarrow}\ \rho_{21}\ \overset{E_+^*}{\rightarrow}\ \rho_{22}\ \overset{E_2}{\rightarrow}\ \rho_{32} \quad \ldots\ldots(3.2c)$$

E_2 is the forward probe field. Processes (a) and (b) contribute to, respectively, the Autler-Townes splitting and the transferred Lamb dip, both of which we observe, but neither causes a two-photon light shift: (a) is too resonant (there is no shift due to E_+, in any order, in the Doppler limit), (b) not resonant enough, for $|\Delta_1| >> \gamma_{21}, \gamma_{32}, \Delta_2$, since the two excited velocity groups then have no significant overlap.

Process (c), however (which is coherent term, and thus absent from the rate equation approximation) does give rise to a shift because E_-^* acts off-resonance, thus moving the gain peaks in an intensity-dependent manner from the double-resonance positions.

For $k_2 << k_1$ the peaks lie at

$$\Delta_2 = \pm \left|\frac{k_2}{k_1}\right| \Delta_1 \left[1 + |\beta|^2 \ (\Delta_1^2 + 2\gamma^2)/(\Delta_1^2 + \gamma^2)^2\right]. \qquad (3.3)$$

Here γ is of $\sim(k_1 \gamma_{32}/k_2)$ - i.e. about 20 MHz and 10 MHz for $^{15}NH_3$ and CH_3OH respectively - and $|\beta| = |\vec{E}_+ . \mu_{12}|/2h$. This quasi-dispersion shape is obtained by a Doppler-limit evaluation of term (2c) for $|\Delta_1| >> \gamma_{21}$. Full details of the calculation will be presented elsewhere. This is by no means the only shifting term, but it is the significant one showing all the observed characteristics:

(1) it is <u>positive</u> (peaks move apart)
(2) it is <u>intensity dependent</u> (linear in this approximation),
(3) it has width in Δ_1 of $\sim \gamma$ rather than γ_{21} (of $\sim$ 1 MHz),
(4) it has the correct magnitude - the maximum departure in equation (3) of Δ_2 from the linear term occurs at Δ_1 of $\sim \gamma$; the measured increase in the splitting for $^{15}NH_3$ of a factor of 2 (Fig 3.2) implies then that $|\beta|$ is of $\sim \gamma$ which is similar to the criterion [37] required for our observation of the Autler-Townes splitting (Fig 3.4). We do not see the latter for CH_3OH and the two-photon light shift is considerably smaller (Fig 3.3). We believe then that the two-photon light shift is demonstrated by our data, but we have not attempted a quantitative fit to (3). This is because our data are read from a PZT, i.e. are <u>length</u> and not frequency measurements. The frequency and length splittings are related

$$\frac{\delta L}{L} = \frac{\delta \nu}{\nu} + \frac{\delta n}{n} \qquad (3.4)$$

A refractive index <u>increase</u> δn in tuning from the low-frequency to the high-frequency peak would thus mimic an increase in splitting. Now at, e.g. the lower frequency, the counterpropagating (resonant) excited molecules contribute large gain and negligible refraction: the co-propagating molecules contribute small gain and a <u>negative</u> refractive index (because of population inversion). A rough calculation indicates that the effect is significant. Because the dispersion is slaved to the gain, however, which in turn is slaved to the cavity losses, we can see that this pseudo-shift should not depend on the molecular species or on the pump power, whereas our shift data is strongly dependent on both. Nevertheless, unambiguous identification of the two-photon light shift demands direct frequency measurements. The system which is being used for the direct frequency measurements of the deviations described is shown in Fig 3.5 Work is in progress to complete the measurements and will be reported at a later stage. As shown, the system is as for the original experiment but with the addition of a second optically pumped submillimetre chain for reference purposes.

CHAPTER IV

METALLIC MESH TECHNIQUES FOR THE SUBMILLIMETRE REGION.

4.1 INTRODUCTION

The use of metallic mesh in submillimetre work is necessary due to the excessive absorption experienced by other materials. Measurements have been made on the transmission characteristics of the two types of mesh available, "inductive" and "capacititive". The application of mesh in filtering throughout the 50 μm to 1 mm region of the spectrum is well documentated [38] and in this report some further developments in the area of filtering are described. The low temperature performance (< 4 K) of a Low Pass type filter is described.

4.2 THEORY

Two types of metallic mesh are described within this report. The first is termed "inductive", and is a periodic array of holes in a thin metal foil of some finite thickness, and the second, "capacitive" is a periodic array of metal squares supported by some substrate. The description inductive and capacitive come from an analogy with trasmission line equivalent circuits as shown in Fig 4.1. The holes (or squares) are usually square and the subsequent $\pi/2$ symmetry eliminates any polarization effects.

The following is essentially a summary of that given by two separate workers [39,40].

A plane electromagnetic wave incident on such structures will cause surface currents and charges to be set up in the metal and these act as secondary souces of electromagnetic radiation. In turn these secondary sources give rise to zero order transmitted and reflected waves of equal amplitude, and after scattering the original wave and the zero order transmitted wave superpose to give the total transmitted wave. Both types of mesh are characterised by two parameters which are: the mesh periodicity (g) and the spacing betwen the squares, 2a, and are represented in Fig 4.2

If the zero order reflection coefficient has a complex amplitude $r(\omega)$, then we describe the transmitted wave amplitude by the fundamental relation,

$$t_I(\omega) = 1 + r_I(\omega) \qquad (4.1)$$

If losses are neglected we can write equation (4.1) as

$$|t_I(\omega)|^2 + |r_I(\omega)|^2 = 1 \qquad (4.2)$$

These expressions are for the inductive mesh, and the expressions

for the capacitive mesh can be derived using the electromagnetic equivalent of Babinets' principle which relates the electromagnetic diffraction fields around a thin, perfectly conducting perforated screen with the fields around the complementary screen. Thus by applying Babinets' principle we have:

$$t_I(\omega) + t_c(\omega) = 1 \tag{4.3}$$

giving
$$t_I(\omega) = r_c(\omega) \tag{4.4}$$
$$t_c(\omega) = - r_I(\omega)$$

where I and c refer to inductive and capacitive respectively.

Absorption has been neglected in the previous description but must be accounted for. Absorption results from ohmic losses of the surface currents flowing in the metallic sections of the grids and also from dielectric losses in the substrate supporting the capacitive mesh.

The absorption is given by,

$$A = |r(\omega)|^2 \quad \left(\frac{c}{\lambda\sigma}\right)^{\frac{1}{2}} f \tag{4.5}$$

where $|r(\omega)|^2$ is the reflectivity, σ is the d.c. conductivity and f is a geometric factor, which is the amount of grid which can conduct current and is given by: for the inductive grid,

$$f_{IN} = g/2a,$$

and for the capacitive grid by,

$$f_{CAP} = \frac{1}{1-2a/g}$$

Looking at equation (4.5) it is evident that in order to reduce the effect of absorption losses, the conductivity should be as high as possible. The most obvious choice would be gold, but the cost is prohibitive. The commonly used metals are copper, nickel and aluminium.

The power transmission is described for a capacitive mesh by,

$$T = \frac{b^2 + z_o\,(\omega/\omega_o - \omega_o/\omega)^2}{(1+b)^2 + z_o{}^2\,(\omega/\omega_o - \omega_o/\omega)} \tag{4.6}$$

where $\omega = g/\lambda$, $\omega_o = g/\lambda_o$ and $b = (c/\lambda\sigma)^{\frac{1}{2}}$. This expression is derived from the equivalent circuit description. The term $(\omega/\omega_o - \omega_o/\omega)$ is the generalized frequency. ω_o is the resonant normalized frequency and λ_o is the frequency at which the capacitive mesh transmission is a minimum (a maximum for the inductive mesh). For an idealized mesh with no losses, this factor, ω_o would be unity.

z_o is known by the characteristic impedance of the mesh and is given by:

$$z_o^c = \frac{1}{\ln \operatorname{cosec}(\frac{\pi a}{2g})} \qquad (4.7)$$

The complimentary relation, $z_o^c . z_o^I = 1$ gives rise to the impedance relation for the inductive mesh.

It is evident that any desired level of reflectivity and transmissivity can be achieved by varying the g and a/g values. Transmission measurements for inductive and capacitive mesh of various g values have been made and are now discussed.

4.3 THE INDUCTIVE MESH

Electroformed inductive mesh was available in the range; 100 lines per inch to 1500 lines per inch. The individual pieces of mesh were stretched over a support ring and secured with flexible collodion, and the transmission profiles were subsequently measured with the aid of a Michelson FS720 Interferometer. Figures (4.3) and (4.4) show the coverage available with the meshes used and also display the characteristic profile of the inductive meshes. The range shown is 0 cm^{-1} to 500 cm^{-1}. The steepness of the slopes is governed by a/g value and this is seen in Fig. (4.4) and (4.5). From the data given by 750 l pi meshes in Fig (4.4) and for the three 1000 l pi meshes presented in Fig. (4.5) it is seen that steeper transmissivity profiles result from larger a/g values.

Calculations using the complimentary relation to equation (4.7) give, in conjunction with the data derived from Figs. (4.3)-(4.5) the a/g values for each mesh.

The complimentary relation is given by

$$z_o^I = \ln \operatorname{cosec} (\pi a/2g) \qquad (4.8)$$

The value, z_o^I was determined from the theoretical fit with the measured profile of the mesh under investigation. Substitution of this value gave the a/g values and these are given in table (4.1).

4.4 THE CAPACITIVE MESH

The capacitive mesh is produced by a photo-etching process with a metal thickness of around $\sim$ 0.2 μm. Capacitive meshes could be produced by the evaporation of metal through an inductive mesh onto a substrate. Figures (4.6) and (4.7) show typical capacitive mesh profiles, indicating the complimentary nature of the two forms of mesh. Table (4.2) presents the necessary details of the capacitive mesh available.

Absorption losses for the metallic mesh have been found to be less than $\sim$ 1%, this being limited by the measuring process.

4.5 LOW TEMPERATURE PERFORMANCE OF A METALLIC MESH LOW PASS INTERFERENCE FILTER IN THE SUBMILLIMETRE REGION.

4.5.1 Introduction

Low Pass or Edge mesh interference filters are finding increased application in space research, submillimetre astronomy and Fourier Transform Spectroscopy. Such applications can however require operation at liquid helium temperatures ($\lesssim$ 4 K) and work has been performed which will show that the Low Pass filter, as described, can be operated at such temperatures.

The low temperature performance of the multielement interference filter has been discussed, with the two-element Fabry-Perot being successfully cycled from room temperatures (300 K) to liquid helium temperatures (1.4 K) [16,41,42].

The Double-Half-Wave design has also been shown to operate without loss of performance at 77 K. [16]. Such filters are constructed with layers of free standing wire mesh ("inductive") separated by metal spacers of thickness $\sim \lambda/2$ μm, where λ is the wavelength of the first order transmission peak.

The Low Pass filter, however, is based on the "capacitive" mesh as described by Ulrich [39,43,44], where squares of metal in a periodic array are either deposited or etched onto a substrate: 2.5 μm Mylar for the filter described. The layers of mesh are separated by $\lambda/4$ μm, so giving an edge at $\sim \lambda$ μm. The theory for the filters described has been well discussed in other works and will not be presented. [16,38]. Low Pass filters constructed with such meshes are currently available for a working range given by 5 cm^{-1} to 225 cm^{-1}.

4.5.2 Experimental Discussion

The method of construction which led to the successful low temperature operation of the Fabry Perot and Double-Half-Wave filters have been applied to the Low Pass filter. That method was to use Invar support rings and TORR-SEAL epoxy as the filter mount. An alternative Low Pass filter which is suitable for low temperature operation has been described where polyethylene acts as the mesh substrate and spacer [45].

The method of construction has been described [46] and will be summarised. A special construction jig which acts as a clamping device is used to hold the two Invar (one upper, one lower) support rings. Meshes and spacers of the desired dimensions are carefully laid out over the lower Invar support ring in the sequence; mesh/spacer/mesh, after which the upper support ring is brought into contact with the mesh stack and tightly clamped. The epoxy is then applied to the two support rings and allowed to set. This method was used to construct the Low Pass filter described.

A design was computed and is given by two capacitive meshes of periodicity 90 μm separated by a single spacer of thickness 17 μm. The constructed filter was measured with a Michelson type Interferometer (Beckman RIIC FS720) and the transmission profile is given in Fig. 4.8(A). The area of transmission in the long wavenumber region is as expected from the theory of a two element Low Pass filter. Additional meshes would be required to complete the blocking region. The filter was cycled a number of times in an Oxford Instruments variable temperature cryostat from 300 K to 77 K and Fig. 4.8(B) shows the resultant profile at 77 K. No degradation in performance has occurred. Figure 4.9 shows the filter at 1.8 K after two cycles from 300 K and shows negligible shift in edge position.

The results have shown that the Low Pass metallic mesh interference filter can be cycled and operated around Liquid Helium temperatures. Such measurements indicate that the Low Pass filter will find more extensive use in the areas described.

4.6 APPLICATION OF MESH TECHNIQUES TO A SUBMILLIMETRE LASER

4.6.1 Introduction

The optical pumping of CH_3OH with the 9P36 CO_2 laser transition has been reported to result in three submillimetre laser emissions at 118.8 μm, 170.6 μm and at 392 μm. The 118.8 μm line however, is the more powerful of the three resulting in the remaining two being not so commonly reported. Identification of weaker emissions, while in the presence of a stronger line is always difficult and a method to ease this task has been devised. This method is to use a blocking filter, based on metallic mesh,

to block the more powerful line external to the cavity, making the identification of other lines easier.

4.6.2 The Use and Design of a Blocking Filter

A simple two element device, similar to that described in the previous section was investigated. Using established design techniques [47] a two element stack of 90 μm meshes separated by a single spacer of 20 μm thickness was constructed and the resulting profile is shown in Fig. (4.10) A good cut-off edge is seen but with incomplete rejection, but this was acceptable since it was only important to ensure that the filter did not have any transmission at 118.8 μm. The filter was measured with a Michelson type Fourier Transform Interferometer, and shows transmission levels of ∿ 80% at 392 μm and ∿ 15% at 170.6 μm.

A large number of modes were observed with the laser operating and the most obvious laser line was the 118.8 μm line. The filter was placed immediately in front of the detector which had the effect of suppressing the powerful line yet on tuning the cavity strong modes still appeared.

An external mesh scanning Fabry-Perot interferometer was used to identify the wavelength of these strong modes, and after repeated tests the presence of the 170.6 μm line was confirmed, although no 392 μm line could be seen. The use of a dielectric guide is thought to be a contributing factor in the difficulty in identifying the 392 μm line, and the use of a metal guide, with its lower losses is suggested. The power level of the 170.6 μm was measured as ∿ 2 mW compared with ∿ 20 mW for the 118.8 μm line.

A method by which one laser line can be suppressed whilst allowing another to be easily identified has been described. This technique could easily be applied to other wavelengths since such filters are easily designed and constructed.

CHAPTER V

CONCLUSIONS AND RECOMMENDATIONS.

We have shown in this report the techniques and methods involved with submillimetre waveguide lasers. Mesh techniques in the submillimetre region have also been described and applications presented.

It is the intention of this Chapter to review the work performed under the contract and to make recommendations which are considered to be worth pursuing. The programme undertaken has resulted in a number of new results and techniques which will be of interest to submillimetre workers.

The cw CO_2 laser commonly used by submillimetre laser labs is of the $^{12}C^{16}O_2$ species. We have shown that by the isotopic substitution of molecules to $^{13}C\ ^{16}O_2$ a new field of work is opened up. The isotopic substitution results in a change in the emission frequencies emitted by the laser, thus by making the change ^{12}C to ^{13}C we are able to increase the number of I.R. frequencies available for optical pumping. The ^{13}C substitution however is not the only available, other isotopes are, ^{12}C, ^{14}C, ^{16}O, ^{17}O, ^{18}O , and these can be combined to give an even larger number of new frequencies. The significance of this increase in new I.R. lines is seen in the optical pumping process described in the report. The emission of submillimetre radiation is dependent on a chance coincidence between a submillimetre absorption frequency and an I.R. pumping frequency. It is evident that if we increase the number of I.R. frequencies then we should have an increased chance of new submillimetre emissions. We have shown this new technique of isotopic pumping is feasible by using $^{13}C^{16}O_2$ optically pumping deuterated forms of methanol and ammonia to produce 17 new submillimetre wavelengths between 78.5 μm and 917 μm.

The natural extension of this work is to use the powerful CO_2 laser at our disposal to investigate a larger number of lasing candidate molecules. This would first be done with an opto-acoustic search with absorptions being investigated for possible lasing action. A research proposal has already been submitted to the US Army European Office for this project (including other avenues of work described in this Chapter).

The isotopic ^{13}C laser has been used to investigate the stability, mode properties and tuning characteristics of the PL_3 pump laser. The output of the $^{13}CO_2$ laser has been observed by a heterodyning technique and it is further intended to determine the effect of the CO_2 laser output on the submillimetre laser action, and this will be performed under the new proposed contract.

The performance of the $^{13}CO_2$ laser with particular attention to cooling effects has been observed. Cooling to $0^{o}C$ has given rise to increases in both output power and the number of I.R. lines observed.

A high power CO_2 laser - the PL_4 has been described, with such a laser being used in the programme of isotopic pumping.

. submillimetre waveguide laser has been designed, constructed and tested to produce a working laser which we have shown can produce submillimetre powers in excess of 1 mW over a large frequency range. The design was flexible to allow a wide range of I/P, O/P couplers and waveguides to be used. The laser has been used in a number of the programmes described within this report, including the fine tuning characteristics of the submillimetre laser.

We have shown non-linearities in the tuning of the submillimetre laser. As described, in general submillimetre laser emission exhibits two gain peaks which are associated with co - and counter-propagating beams in the waveguide resonator. The separation of the peaks - the Doppler splitting - should be linear with pump frequency offset as predicted by rate equation theory. We have shown that dispersion - a nonlinearity in cavity length versus frequency - and two photon light shift effects are present which produce a deviation from that expected by rate equation theory. The measurements taken were from cavity length considerations and in order to determine the relative magnitude of the two effects an additional direct frequency experiment should be carried out in addition to the previous experiment described. The experimental apparatus for this experiment has been described and a report on the results should be available in the near future.

The splitting we observed was with $^{15}NH_3$ and CH_3OH and it was the high efficiency of the transitions at 153 μm and 118.8 μm that enabled us to perform such measurements. With a high efficiency transition it is possible operate with extremely low pump powers and submillimetre laser pressures and this results in the necessary standing wave situation being set up for the experiment.

With the increased interest in optically pumped submillimetre lasers for high resolution laser spectroscopy, heterodyne measurements, frequency synthesis, plasma research and solid state physics it is important to have high frequency stability and spectral purity and the programme undertaken goes part of the way to describe the necessary performance and explain the operation of the submillimetre laser. Further work is required to measure the submillimetre frequency output and stability (as already discussed) and secondly we would require to study rate coefficients for inelastic molecular collisions in the field of the submillimetre laser. No experimental data exists for the rate coefficients and it is proposed to measure individual rotationally inelastic rate coefficients and wall deactivation rate coefficients in an external gain cell.

Mesh techniques have also been investigated. A wide range of "inductive" and "capacitive" type meshes have been characterised, showing the complimentary nature of the two structures. These meshes have been used in simple Fabry Perot configurations as scanning interferometers and were used to determine submillimetre emission wavelengths from our laser.

A low pass blocking filter, based on interference effects has been designed and constructed to block submillimetre wavelengths resulting from cascade type emissions in CH_3OH. In addition to the powerful 118.8 μm line pumped by the 9P36 transition, 2 longer wavelengths are also emitted at 170.6 μm and 392 μm. The filter was used to block the 118.8 μm line outside the cavity to enable easier identification of the remaining lines. This has been shown to be a useful technique for laser line supression.

The low temperature performance (< 4 K) of a mesh low pass filter has been shown for the first time in this programme. The filter was constructed with Invar supports and TORR-SEAL epoxy. Such a result is useful in astronomical observations. Further work on filters with 3 or more elements is now planned to give improved rejection, while retaining the 4 K performance.

A range of materials suitable for use in the submillimetre region have been characterised both at room temperatures and Liquid Nitrogen temperatures. Such materials are necessary for use as window or filter devices.

In conclusion we have investigated a number of techniques and phenomenon in the submillimetre region, but would recommend further studies as described in this report to lead to a fuller understanding of the optically pumped submillimetre laser.

APPENDIX 1

MATERIALS SUITABLE FOR USE IN THE SUBMILLIMETRE REGION

A1.1 INTRODUCTION

The increasing interest in the submillimetre region of the electromagnetic spectrum (40 μm to ∿ 1.2 mm), as seen in the increased number of relevant publications, has led to the demand for more information regarding the materials which are likely to be incorporated within submillimetre systems.

This report brings together a range of materials which have been, or are likely to be used by workers. The materials discussed are: T.P.X., P.T.F.E., Alkythene 11, Fused and Crystal Quartz, Sapphire and Mylar. Material performance at 77 K is also described.

A1.2 EXPERIMENTAL APPARATUS AND DATA

The equipment used to obtain the spectra presented was a Beckman RIIC FS720 Michelson type Interferometer [48] which could be used through the range ∿ 6 cm^{-1} to 500 cm^{-1}. Such a coverage was achieved with a suitable choice of Beamsplitter thickness (Mylar) and Golay detectors (quartz and diamond windows). With such a system, however, spectra recorded between 6 cm^{-1} and 10 cm^{-1} was noisy. The optical arrangement of the interferometer is shown in Fig. A1. The transmission profiles were recorded with the samples placed at position A, as shown in Fig. A1.

Infrared spectra described were obtained using a Perkin Elmer 580 spectrometer.

Various discussions have been presented on materials [49-53], and this appendix is intended to compliment such works. All materials described are readily available from the suppliers given in Table A1.

Two samples of T.P.X. (4-methyl-pentene-1) have been used as windows for the submillimetre laser in our laboratory. The thicknesses used were as detailed in Fig. A2. The general transmission profiles are identical but for a difference in levels. The transparency of the material in both the visible and sub-millimetre region makes it an excellent candidate for window or lens use. The 10 μm transmission is effectively zero.

Figure A3 shows the profile of a 2 mm thick sample of P.T.F.E. (polytetra-flourethylene). The edge around 200 cm^{-1} (50 μm) is a useful feature, displaying characteristics similar to commercially available low pass filters [54].

Cooling to liquid Nitrogen temperatures (77 K) had little effect on the edge or overall transmission.

Thinner samples have been investigated, ranging from 150 μm to 950 μm and the effect of thinning the material is shown in Fig. A4 for 250 μm and 950 μm samples. The insert shows the I.R. transmission for the two thicknesses (the transmission of the 2 mm sample at 10 μm being zero).

A not so commonly used low density polyethylene is Alkythene 11, which is partially opaque in the visible. A 5 mm thick sample resulted in the transmission shown in Fig. A5, with the insert showing the I.R. performance.

Two widely used materials are Fused and Crystal quartz and although they have been extensively discussed [51-53] they are included for completeness. A 1 mm sample of fused quartz (Suprasil 2) was measured, with the resultant profile shown in Fig. A6. Cooling to 77 K resulted in little change in profile.

Fig. A7(a) shows the transmission of a 1 mm thick sample of crystal quartz (z-cut), with the prominent absorption around 130 cm^{-1} being seen. The sample was cooled to 77 K (b), resulting in a shift of the absorption band to longer wavenumbers. Such a shift was in accordance with a previous discussion. Both fused and crystal quartz are visibly transparent, with 10 μm blocking being effective in both.

At room temperature sapphire has a transmission profile as shown in Fig A8(a). At 77 K however the transmission region opens out as shown in Fig A8(b). The curves shown are for a 1 mm sample. As for quartz, this material was visibly transparent, with 10 μm being blocked.

Finally, two thicknesses of Mylar (Melinex), 2.5 μm and 12 μm have been measured with their profiles being seen in Fig. A9. Such materials are commonly used as beamsplitters and substrates for "capacitive" type mesh [39].

LITERATURE CITED

1. Patel, C.K.N., (1968), "Lasers", ed. by Levine, A.K., (Edward Arnold (Publishers) Ltd, London), vol. 2, Chapter 1.

2. Svelto, O (1976), "Principles of Lasers" (Heyden/Plenum Press, New York), pp 210-213.

3. "PL_3 Operating Handbook", (1977), (Edinburgh Instruments Ltd., Edinburgh, U.K.).

4. Sverdlov, L.M., Kovner, M.A., Krainov, E.P., (1974), "Vibrational Spectra of Polyatomic Molecules", (Halstead Press, Wiley and Sons, New York).

5. Freed, C., Ross, A.H.M., O'Donnell, R.G. (1974), J. Mol. Spectrosc., vol. 49, p.439.

6. Siddoway J.C. (1967), J. Appl. Phys., vol 38, p.2629.

7. Smith A.L.S., Moffat S., (1979), Opt. Commun., vol 30, No. 3 p.213.

8. PL_4 Operating Handbook (Edinburgh Instruments Ltd., Edinburgh, U.K.) (1980).

9. Chang T.Y., Bridges T.J. (1970), Opt. Commun., Vol. 1, No. 9 P.423.

10. Danielewicz, E.J., Galantowicz, T.A., Foote F.B., Reel R.D., Hodges D.T. (1979), Opt. Lett., Vol 4, No. 9 p 280.

11. Hodges D.T., Hartwick T.S., (1973), Appl. Phys. Lett., vol. 23, No. 5

12. Wood R.A., Davis, B.W., Vass A., Pidgeon C.R., (1980), Opt.Lett., vol. 5, No. 4, p 153.

13. Davis, B W., Vass A., Pidgeon C R., Allan G.R., (1981), Opt. Commun., vol 37, No. 4, p.303.

14. Wood R.A., Vass A., Pidgeon C.R., Firth W.J., (1980), Opt. Commun, vol 35, No. 1, p.105.

15. Pidgeon C.R., Firth W.J., Wood R.A., Vass, A., Davis B.W., (1981) Int. J. Infrared and Millimetre Waves, Vol. 2, No. 2, p. 207.

16. Davis B.W. PhD Thesis, Heriot-Watt University, Edinburgh U.K. (1980).

17. Walzer,K., Tacke M., Busse G., (1979), Infrared Phys. Vol. 19, p.175.

18. Marcatelli E.A.J., Schmeltzer R.A., (1964), Bell System Tech. J. Vol. 43, p.1783

19. Kneubühl F.K., Affolter E. (1979) "Infrared and Sub-Millimetre Waves", ed. Button K.J. (Academic Press, N.Y.) vol. 1, Chapter 6, p.235.

20. Blaney T.J., National Physical Laboratory, Teddington, U.K. (Personal Communication).

21. Chang T.Y., Lin C., J. Opt. Soc. Am., (1976), vol. 69, p.362.

22. Wood R.A., Vass A., Pidgeon C.R., Colles M.J., Norris B., (1980), Opt. Commun. vol. 33, p.89.

23. Norris B., Colles M.J., Wood R.A., Vass A., Pidgeon C.R., proc. European Conf. Opt. Systems and Applications, Utrecht, 1980.

24. W.J. Firth, R. Salomaa and P.E. Toschek, 4th UK National Quant. Elec. Conf., Edinburgh: "Laser Advances and Applications" (John Wiley and Sons, New York, 1980).

25. R. Keil and P.E. Toschek, 3rd Int. Conf. on Laser Spectroscopy, Jackson Hole, Wyo., p. 306 (Eds. Hall and Carlsten) Springer-Verlag (1977).

26. C. Cohen-Tannoudji, F. Hoffbeck and S. Reynaud, (1978) Opt. Commun., 27, 71.

27. see for example: A. Schabert, R. Keil and P.E. Toschek, Appl. Phys., 6, 181 (1975); C. Delsart and J.c. Keller, Opt. Commun., 16, 388 (1976).

28. D. Seligson, M. Ducloy, J.R.R. Leite, A. Sanchez and M.S. Field, IEEE J. Quant. Electron., QE-13, 468 (1977).

29. R.J. Temkin, IEE J. Quant Electron (1977) QE-13, 450.

30. J. Heppner and C.O. Weiss, (1977) Opt. Commun., 21, 324

31. J. Heppner, C.O. Weiss and P. Plainchamp, Opt. Commun., 23, 381 (1977); G. Koepf, Proc. Heterodyne Systems Conf., Williamsburg, March 28-30 (1980).

32. F.R. Peterson, K.M. Evenson, D.A. Jennings and A. Scalabrin, IEEE J. Quant. Electron., QE-16, 319 (1980).

33. Duxbury, G., Herman H, (1978), J. Phys. B11, p935, Inguscio M., Moretti, A., Strumia F., Optics Commun., 30 (1979), 355; 32 (1980) 87.

34. Heppner J., Weiss C.O., Plainchamp P., 1977, Opt. Commun. Vol. 23, p.381

35. Bradley C.C., Jones R.G., Birch J., Duxbury G., (1970), Nature, Vol. 226, p 941.

36. Feldman B.J., Feld M.S., (1972), Phys. Rev., A5, p.899.

37. Salomaa R., Stenholm S., (1976), J. Phys., B9, p.1771.

38. Holah, G.D. , Smith S.D. (1977), J. Phys. E: Scientific Instruments, Vol. 10 p.101.

39. Ulrich R. (1967), Infrared Physics, vol. 7, pp 37-55.

40. Marcuvitz N., (1951), "Waveguide Handbook", MIT Rad. Lab. Series, (McGraw-Hill).

41. Holah G.D., Davis B., Morrison N.D., (1978), Infrared Physics, Vol. 18, p 621.

42. Holah G.D., Morrison N.D., Goebel J.G., (1979), Appl. Opt. Vol. 18, 3526.

43. Ulrich R., (1967), Infrared Physics, Vol. 7, p. 65.

44. Ulrich R., (1968), Infrared Physics, Vol. 7, p.1987.

45. Whitcomb S.E., Keene J., (1980), Appl. Opt., vol. 19,p.197.

46. Holah G.D., Davis B., Morrison N.D., (1979), Infrared Physics, Vol. 19, p.639.

47. Holah, G D., Auton J.P., (1974), Infrared Physics, Vol 14, p.217.

48. Beckman RIIC Ltd., "IR 720 FIR Spectrometer System Instruction Manual", Issue One (1973).

49. Kimmitt M.F., "Far-Infrared Techniques", Pion Ltd., London, (1970).

50. Melchiorri B., Natale V., Fiscella B. and Lombardini P., Infrared Phys., 16, p.253 (1976).

51. Roberts, S and Coon D D., J. Opt. Soc. Am, 52, No. 9 (1962).

52. Russell E.E., and Bell E.E., J. Opt. Soc. Am., 57, No. 3 (1967).

53. Loewenstein E.V., Smith D.R. and Morgan R.L., Appl. Opt. 12, No. 2 (1973).

54. Cambridge Consultants Ltd., Science Park, Milton Road, Cambridge, CB4 4DW, U.K.

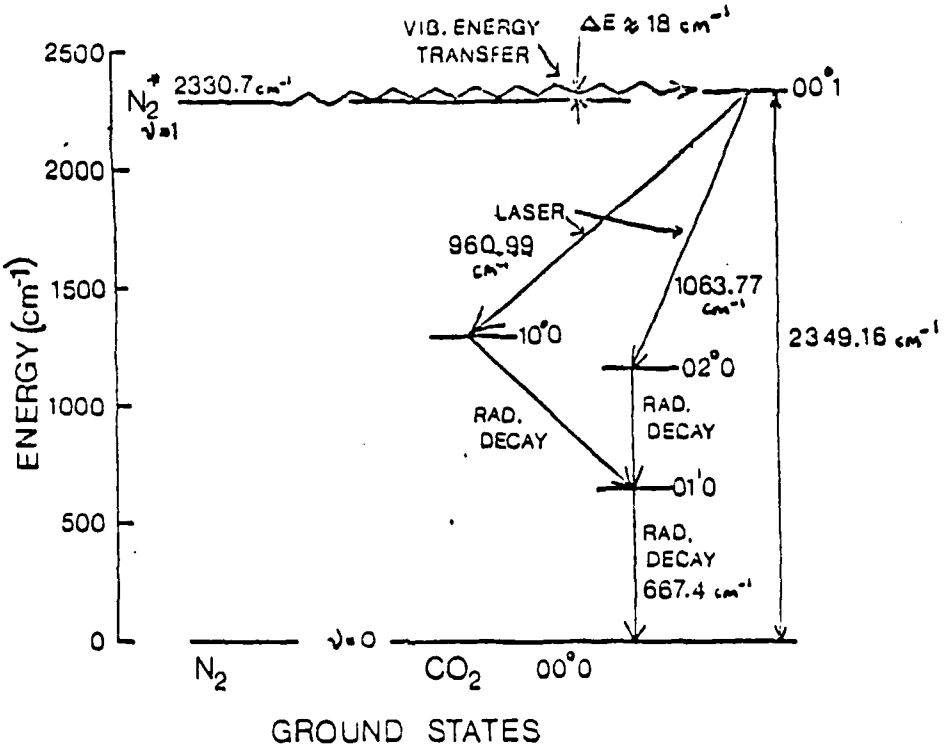

Fig. 1.1 Partial Energy diagram of N_2 and CO_2 showing laser transitions at 9.3 μm and 10.6 μm.

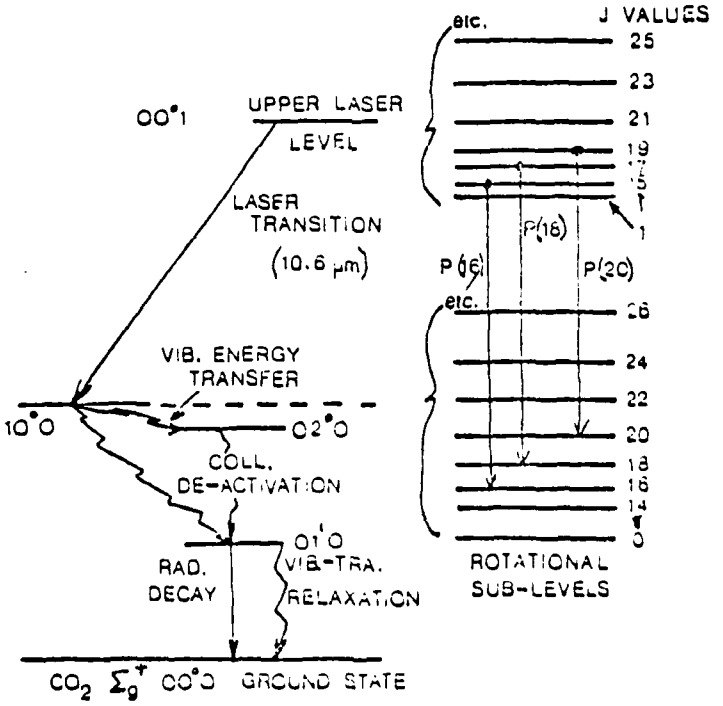

Fig.1.2 Detailed laser transition diagram for the $00^{0}1$ - $10^{0}0$ band (including rotational levels).

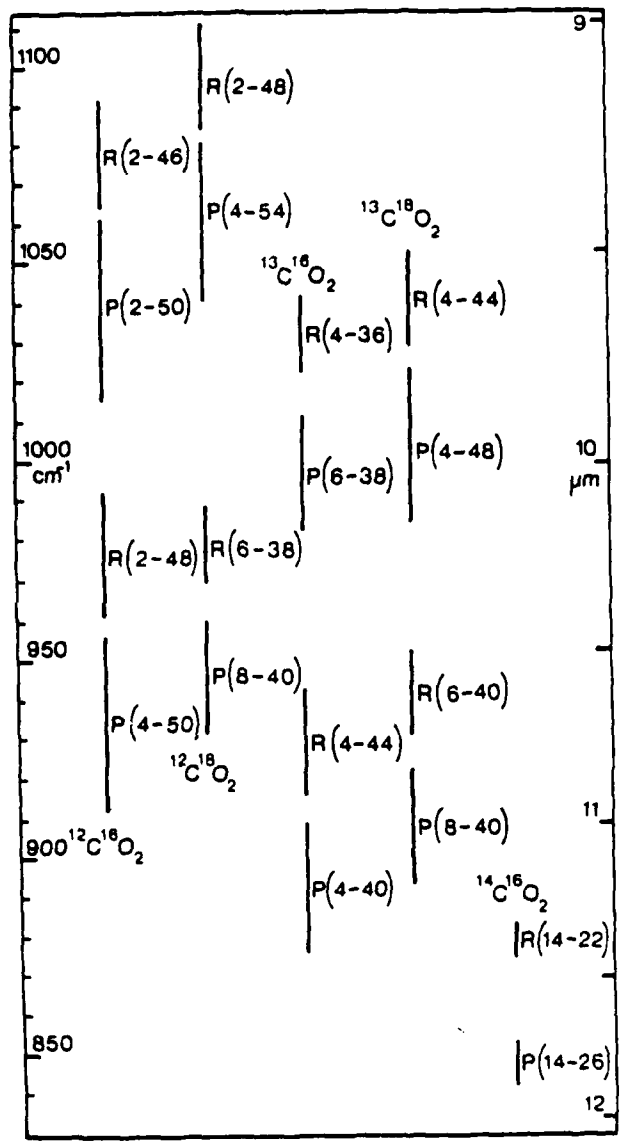

Fig. 1.3 Observed frequency ranges of isotopic CO_2 laser bands.

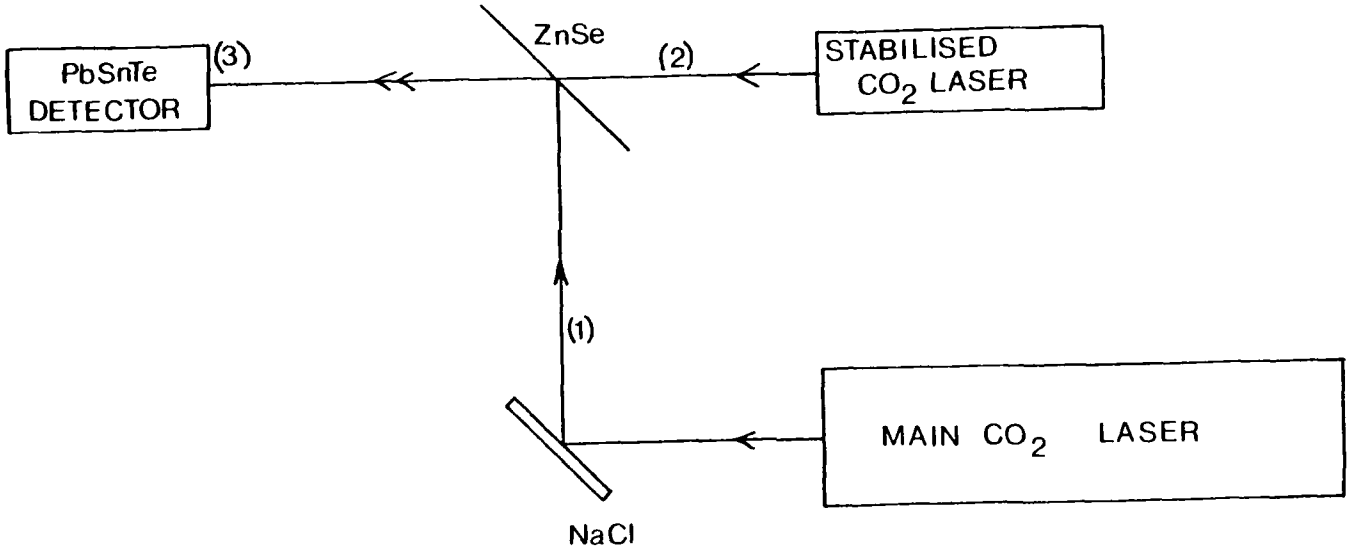

Fig 1.4 Experimental arrangement of the CO_2 heterodyning system.

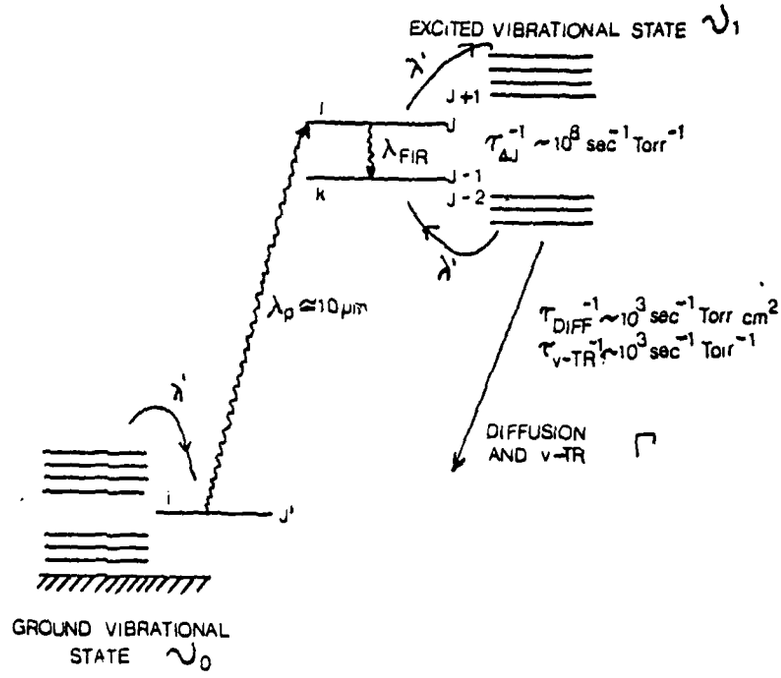

Fig.2.1 Schematic partial energy diagram of a polar molecule.

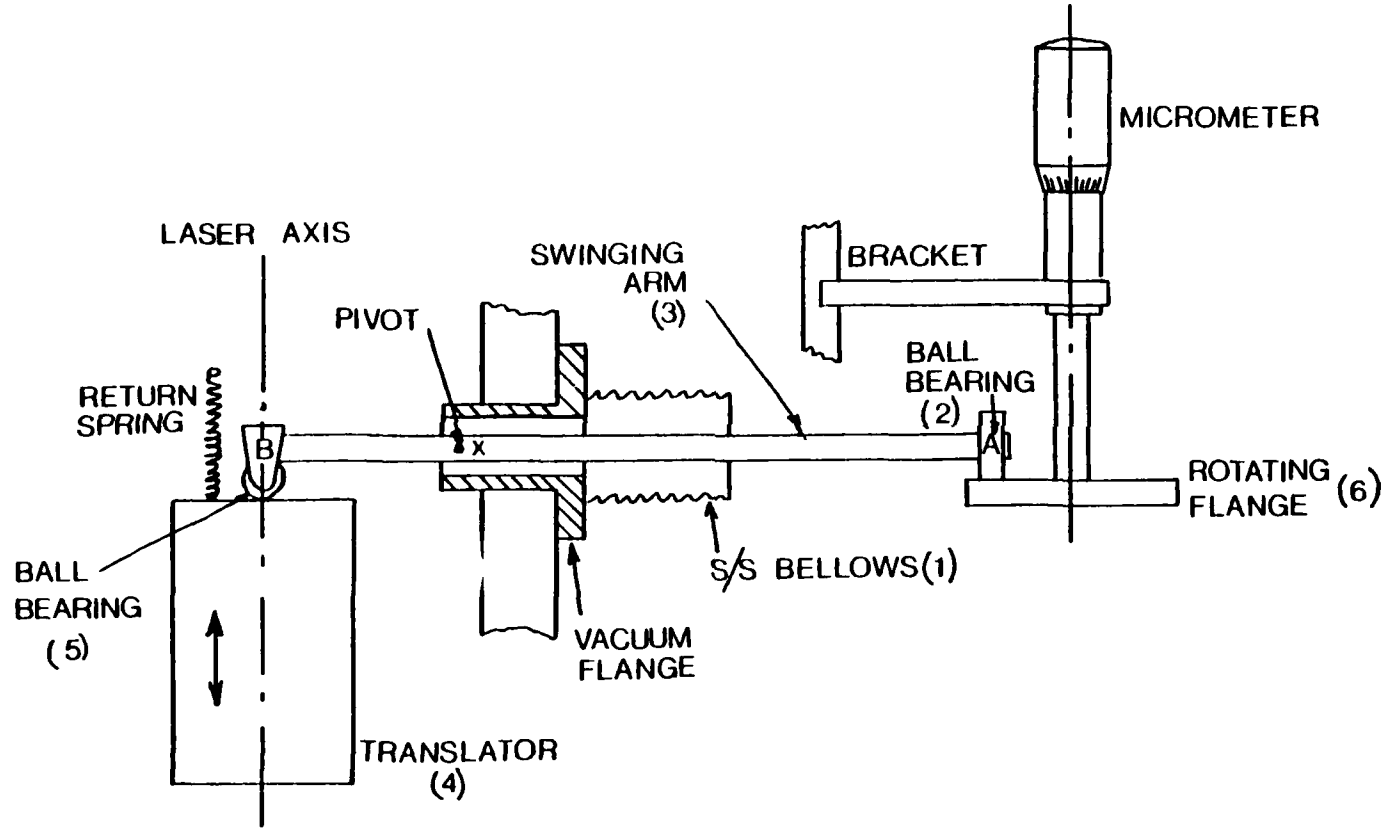

Fig.2.2 The mirror translation system.

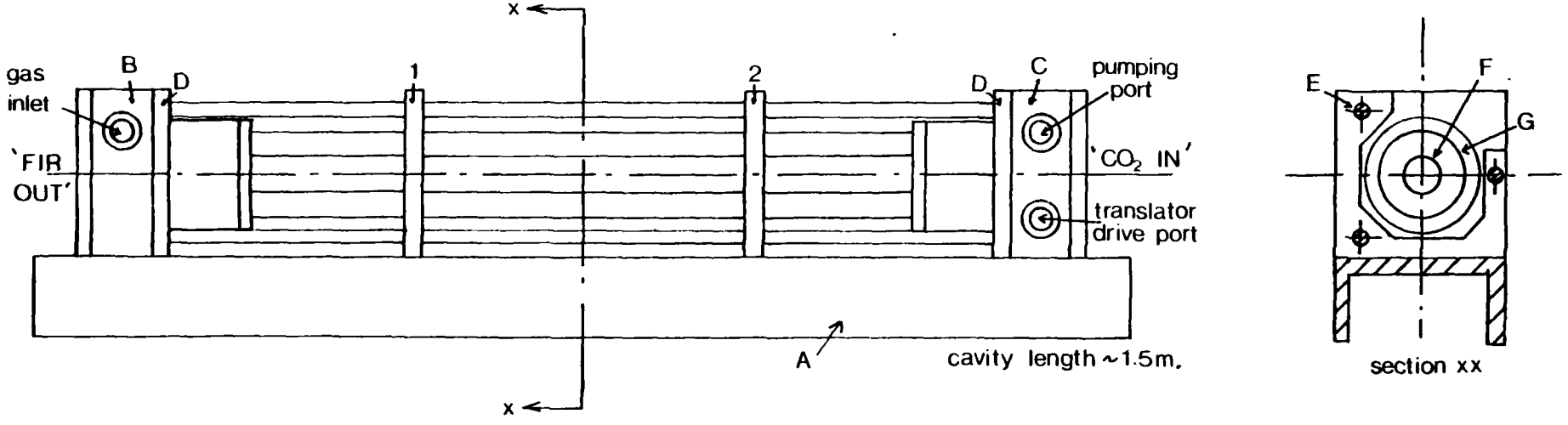

Fig. 2.3 Schematic diagram of laser.

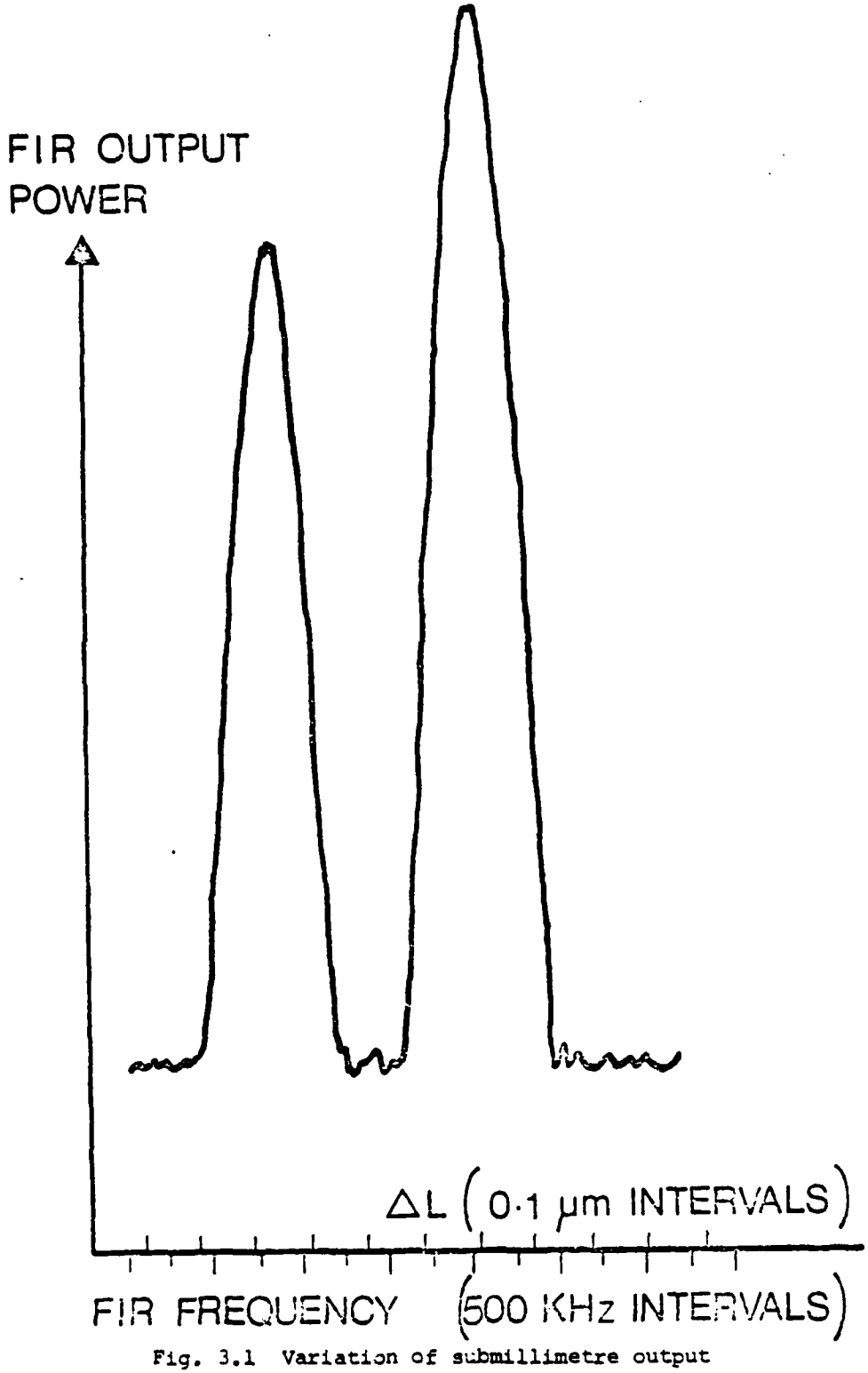

Fig. 3.1 Variation of submillimetre output power (λ = 152.9 μm) in EH_{11} mode as resonator length is varied (ΔL). Lower scale shows submillimetre frequency scale deduced from the Fabry-Perot relationship $^{13}CO_2$ 10R(18) laser offset frequency 22.7 $\pm$ 0.5 MHz.

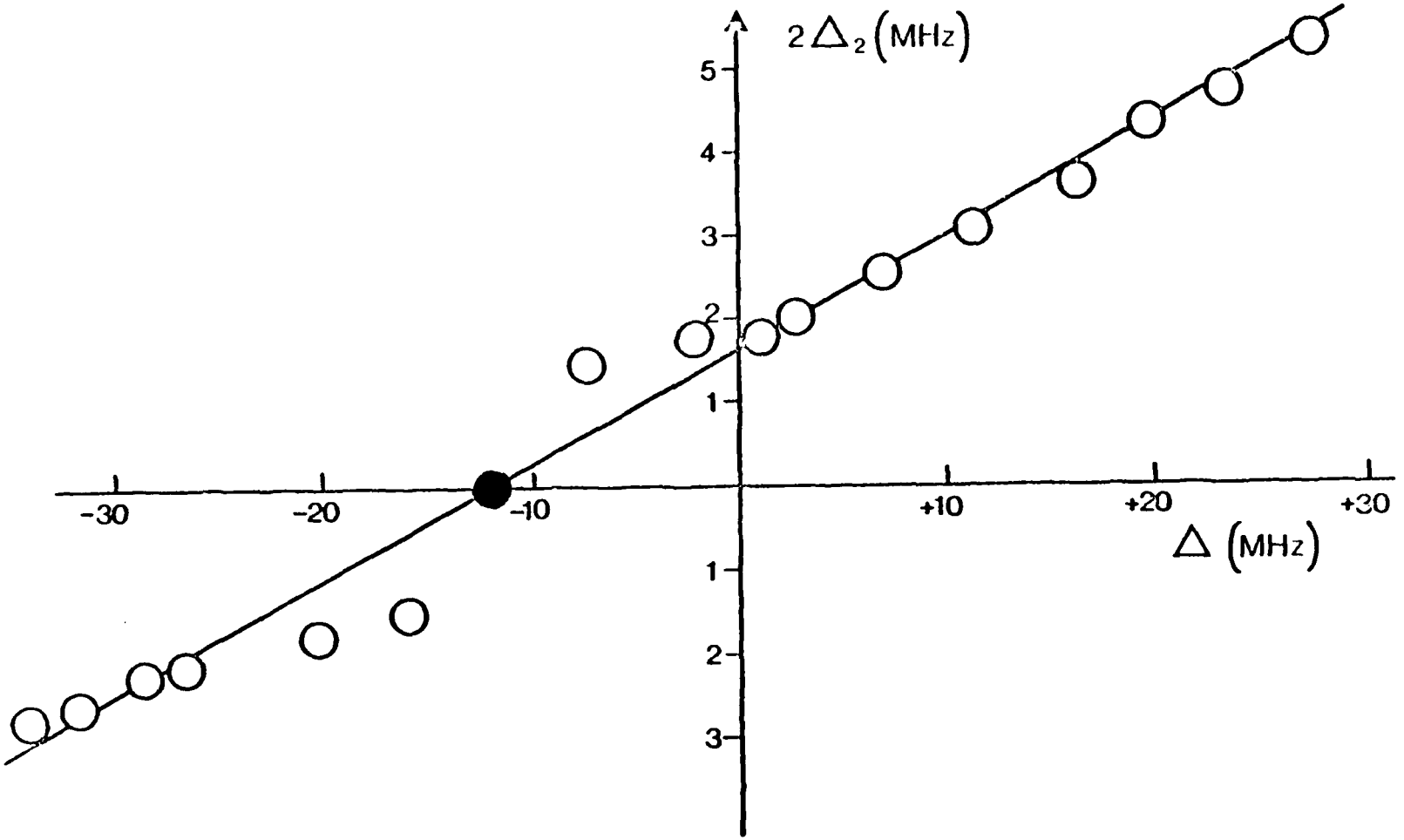

Fig 3.2 Observes splitting of $^{15}NH_3$ (λ = 152.9 μm) submillimetre gain maximum $|2\Delta_2|$ as a function of $^{13}CO_2$ 10R(18) pump frequency offset; the pump power and submillimetre laser pressure were set just below the values required for the onset of Autler-Townes Splitting. Circles show the experimental data, and the solid line the slope expected from rate equation theory.

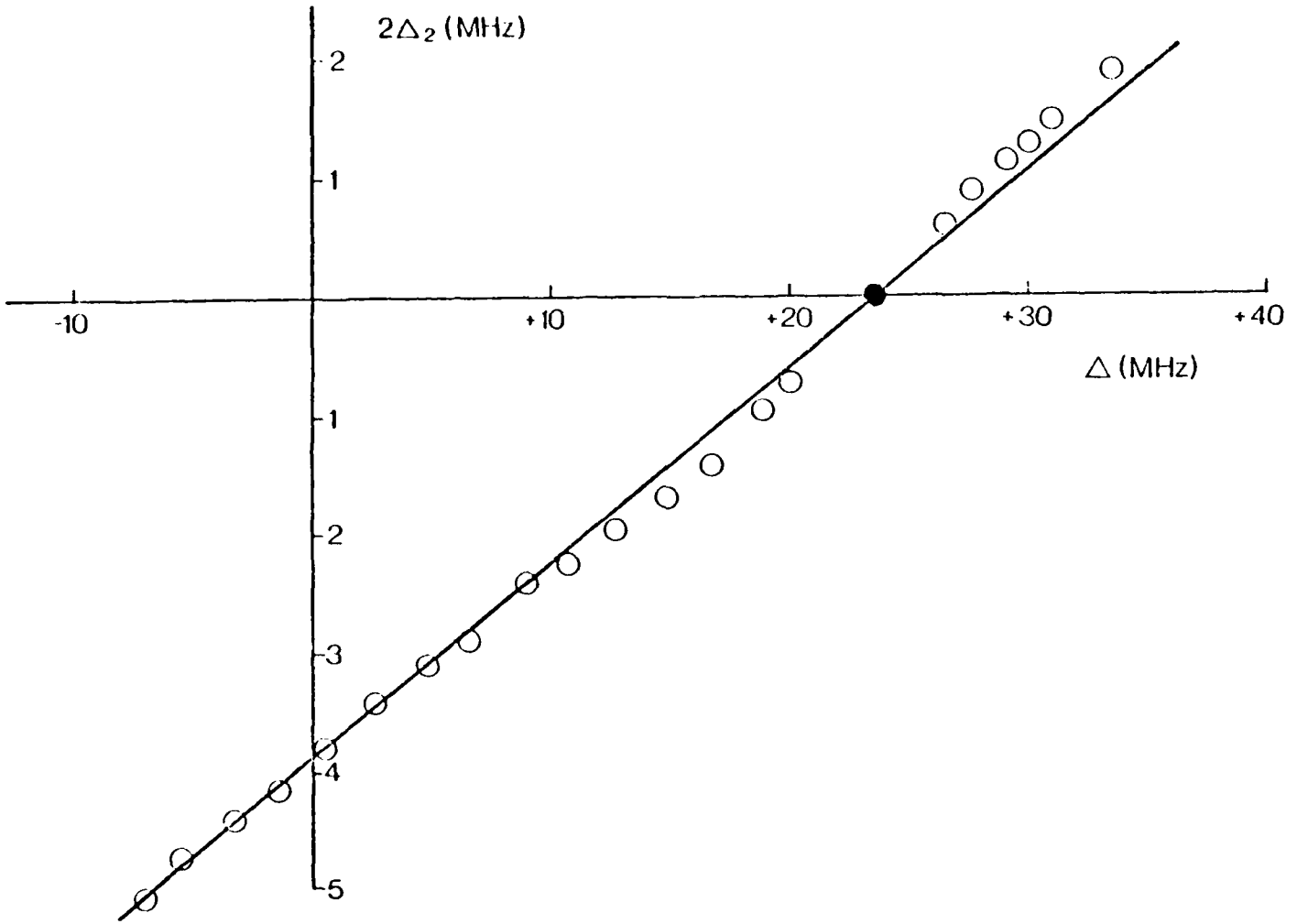

Fig. 3.3 Observed variation of $|2\Delta_2|$ with Δ for CH_3OH (λ = 118.8 μm) pumped by $^{12}CO_2$ 9P(36) under the same conditions as Fig. 3.2.

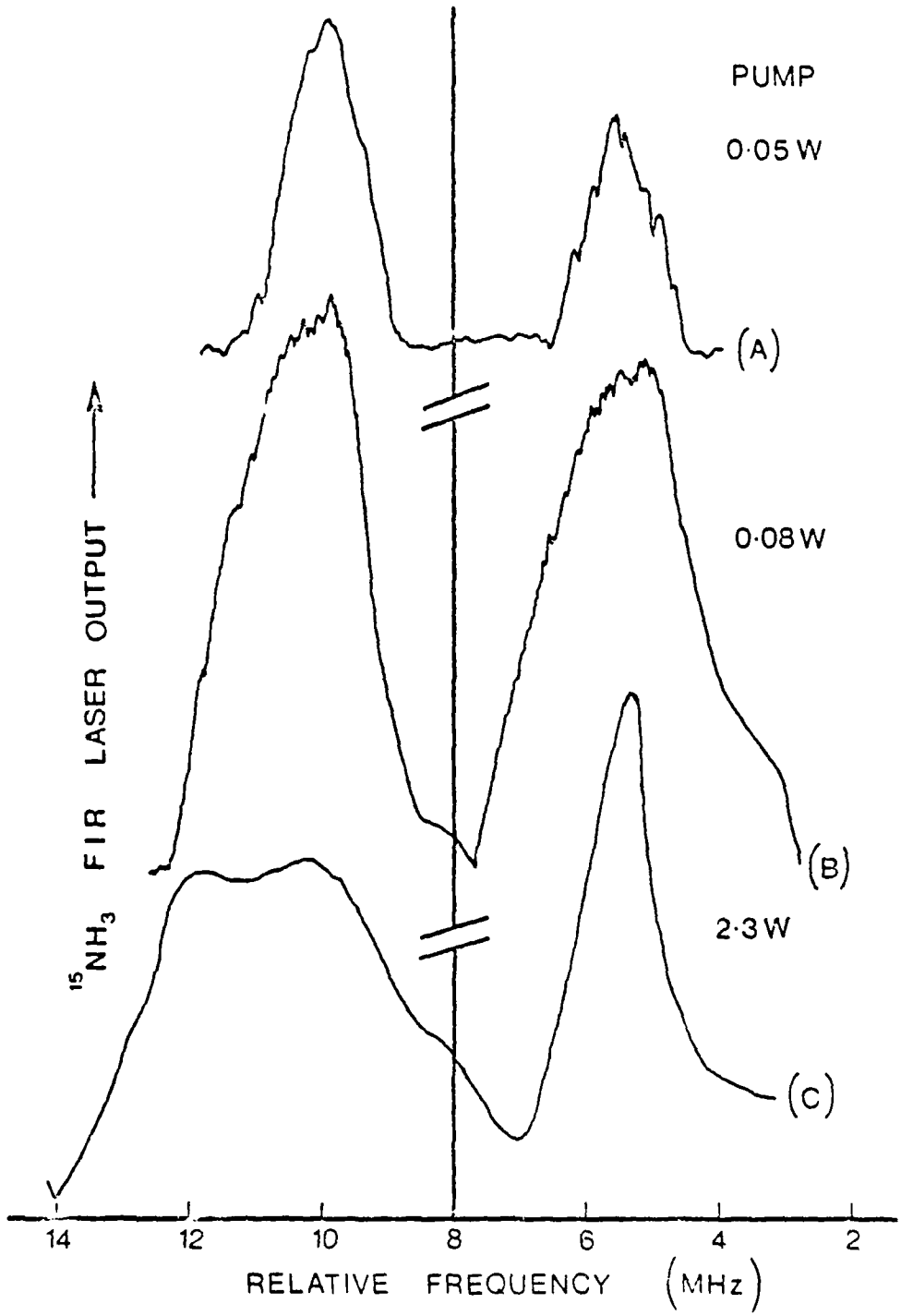

Fig 3.4 $^{15}NH_3$ (λ = 152.9 μm) laser EH_{11} mode output power variation (arbitrary units) as resonator length is varied for $^{13}CO_2$ 10R(18) laser input power levels of 0.05 W (A), 0.08 W (B) and 2.3 W (C). Lower scale shows submillimetre frequency scale deduced from the Fabry-Perot relationship.

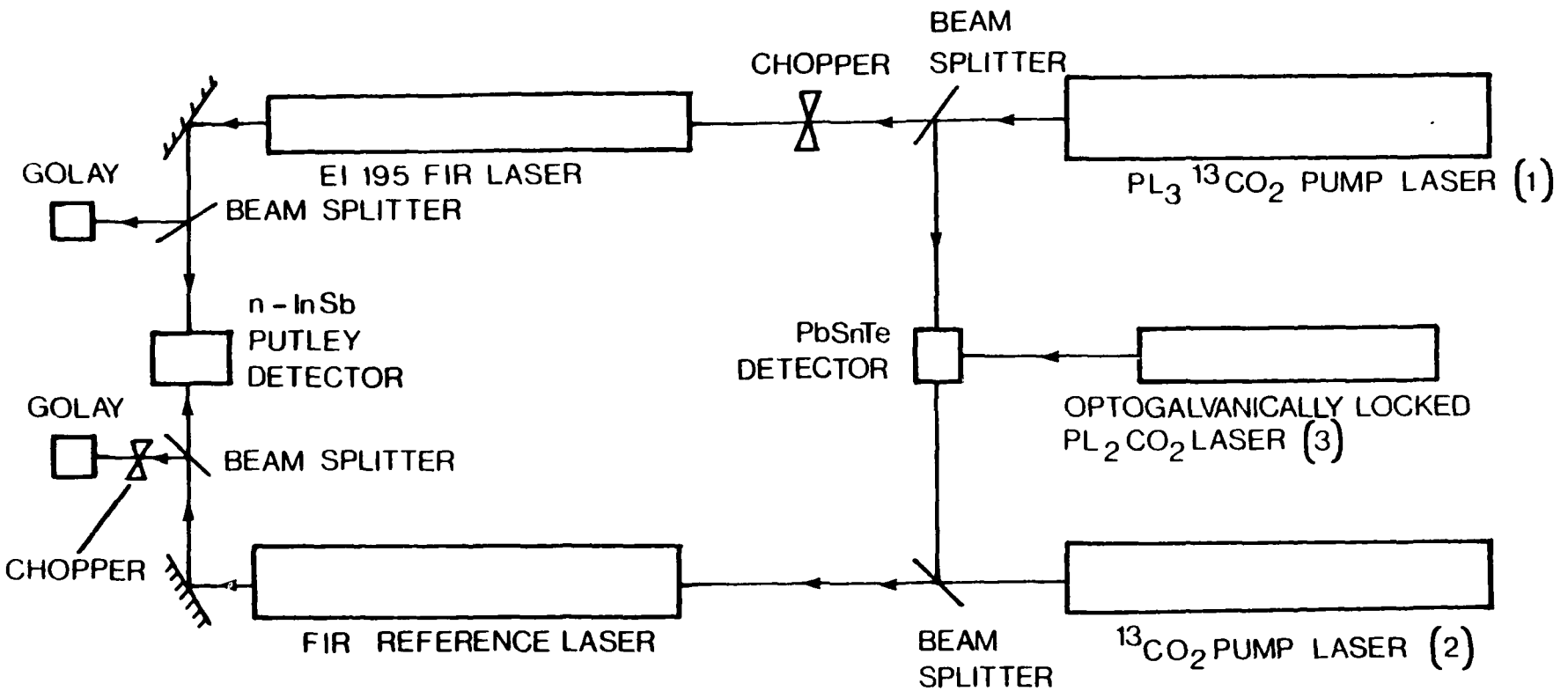

Fig. 3.5 Submillimetre heterodyne system for direct frequency determination.

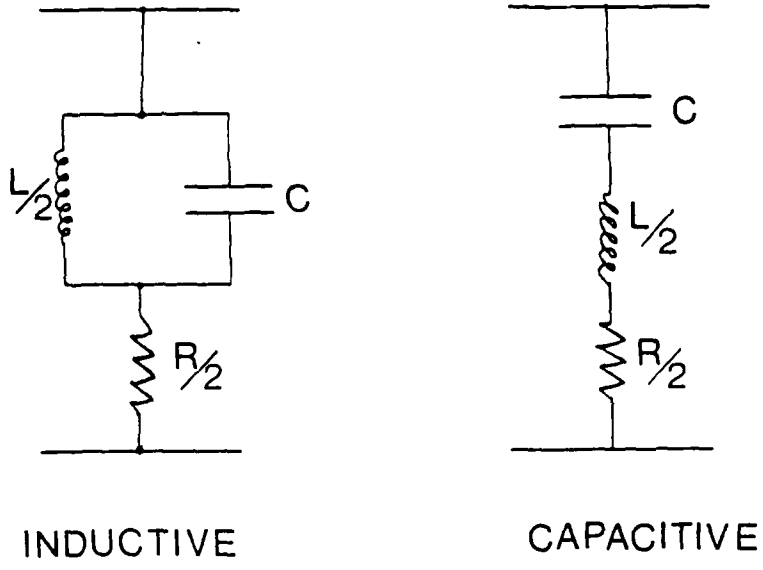

Fig.4.1 Transmission line equivalent circuits and capacitive mesh.

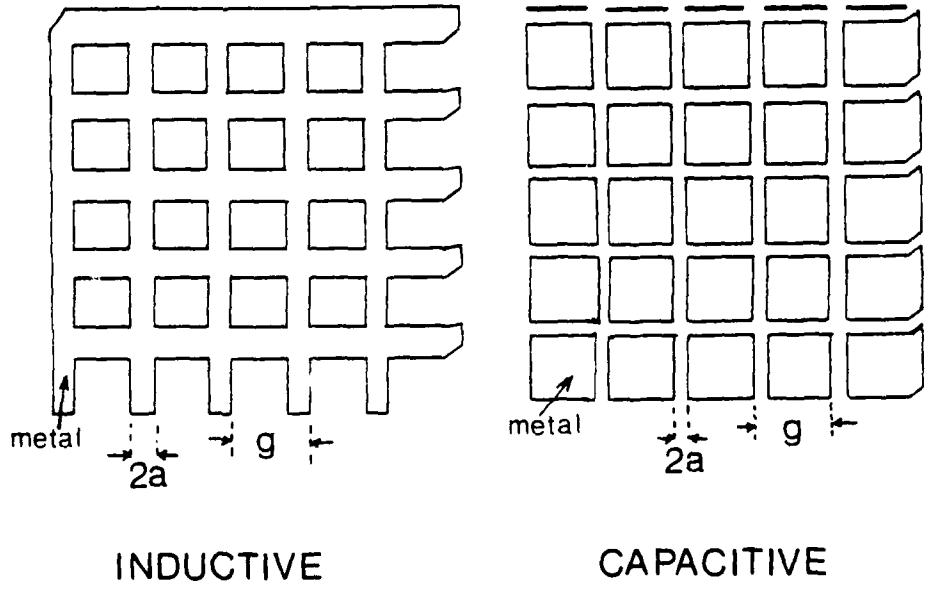

Fig. 4.2 Geometrical parameters of inductive and capacitive mesh.

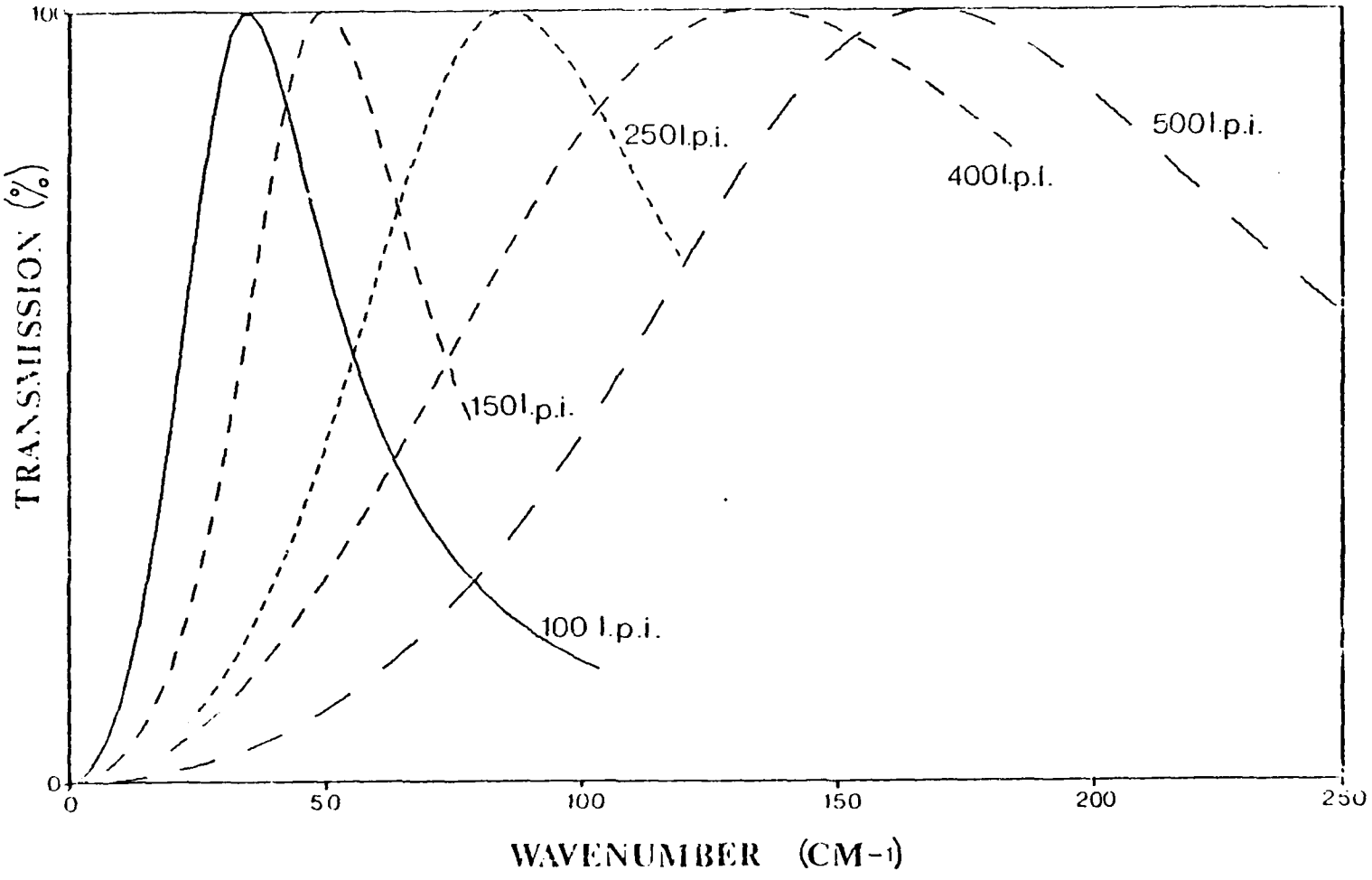

Fig. 4.3 Transmission profiles of inductive meshes, 100 L.P.I. to 500 L.P.I.

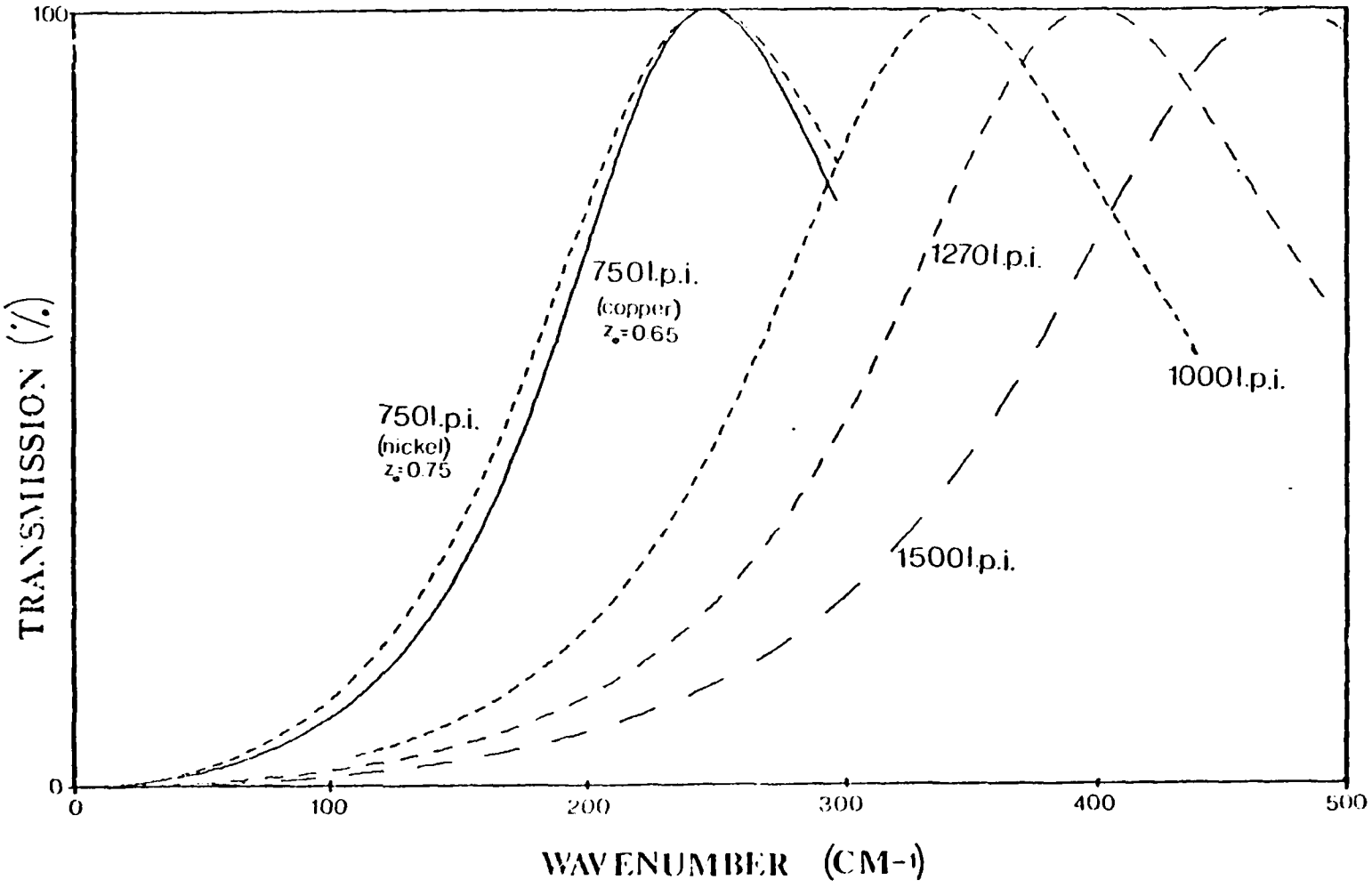

Fig. 4.4 Transmission profiles of inductive meshes, 750 L.P.I. to 1500 L.P.I.

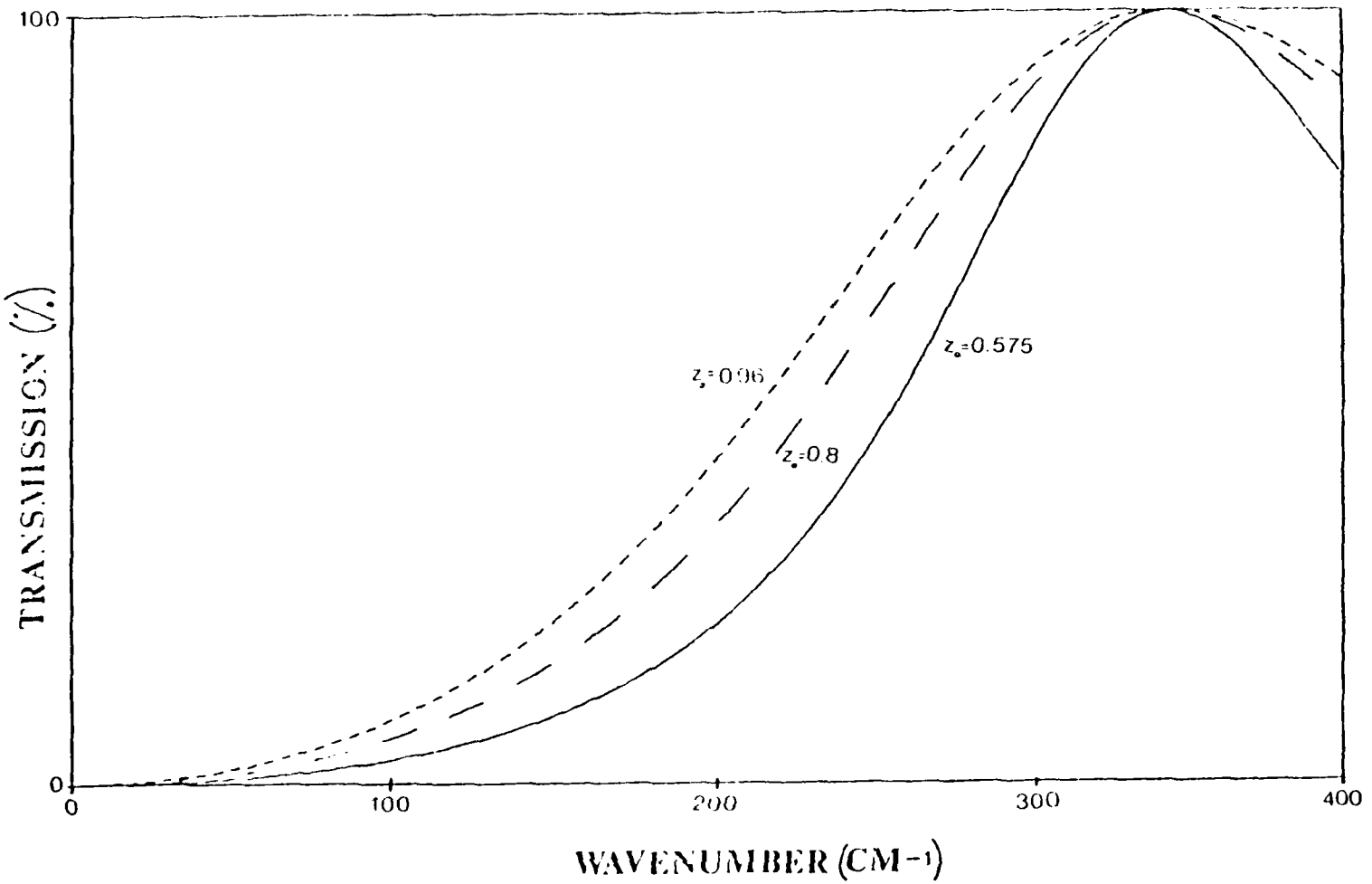

Fig. 4.5 Comparison of 1000 L.P.I. inductive meshes with different z_o values.

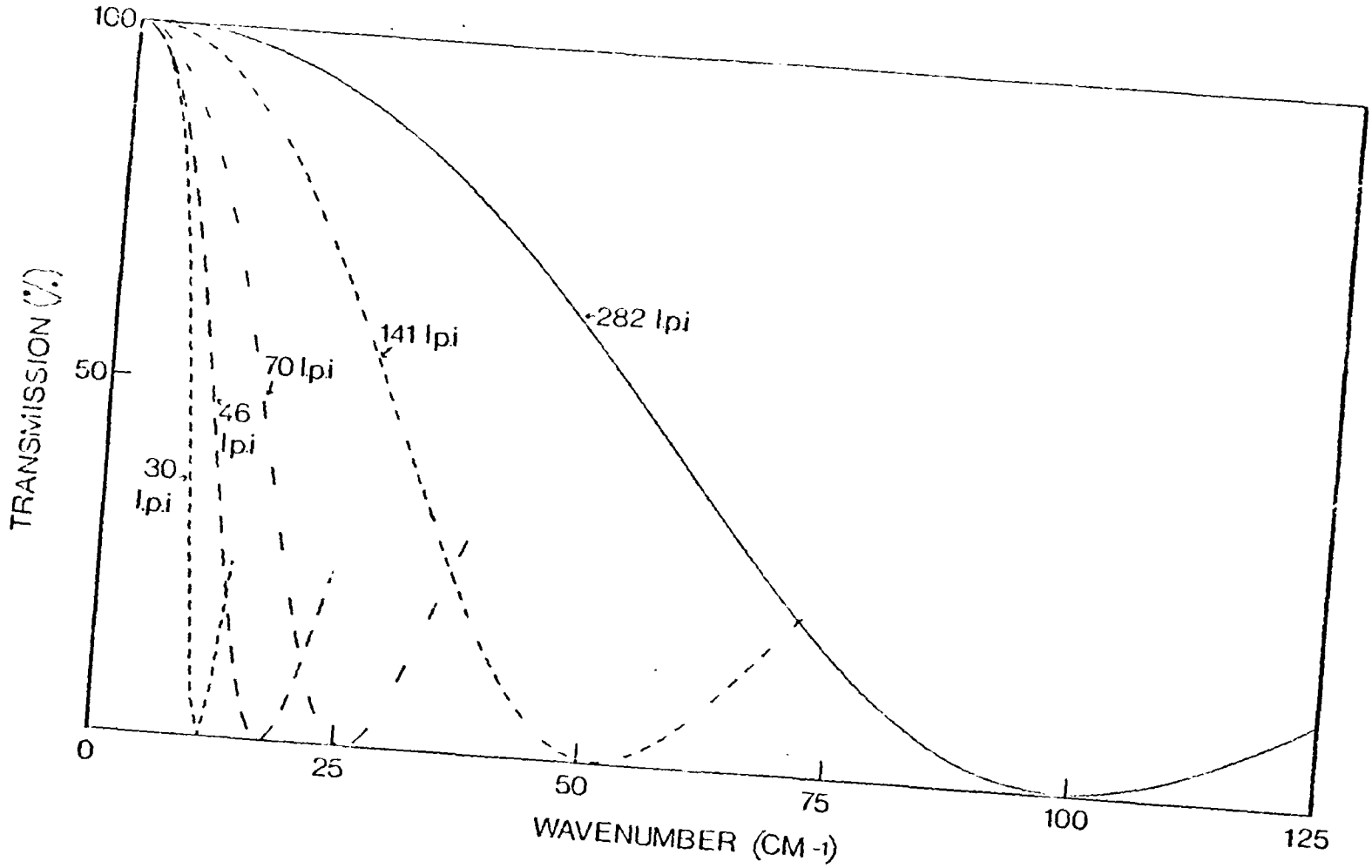

Fig. 4.6 Transmission profiles of capacitive meshes, 30 L.P.I. to 282 L.P.I.

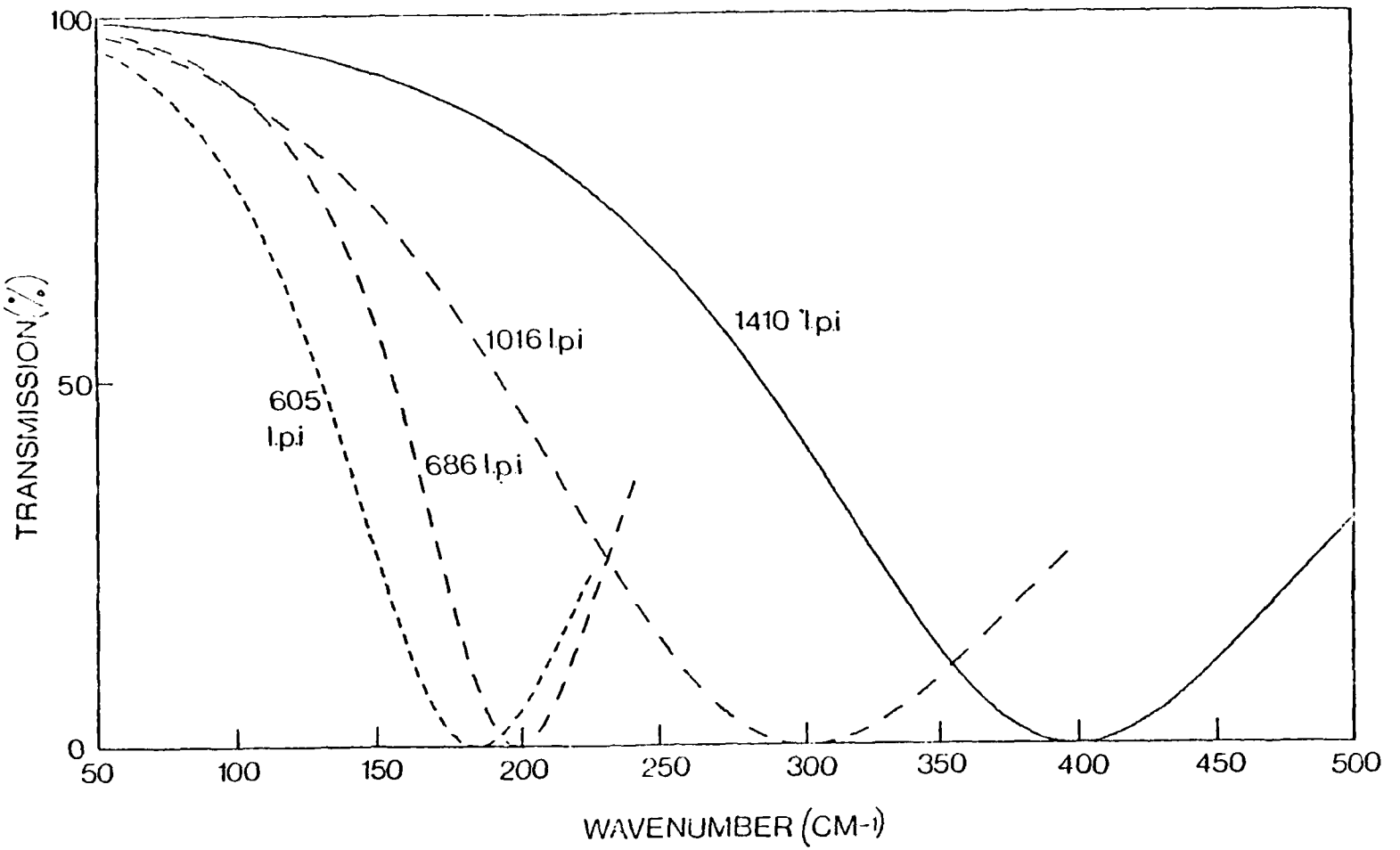

Fig. 4.7 Transmission profiles of capacitive meshes, 605 L.P.I. to 1410 L.P.I.

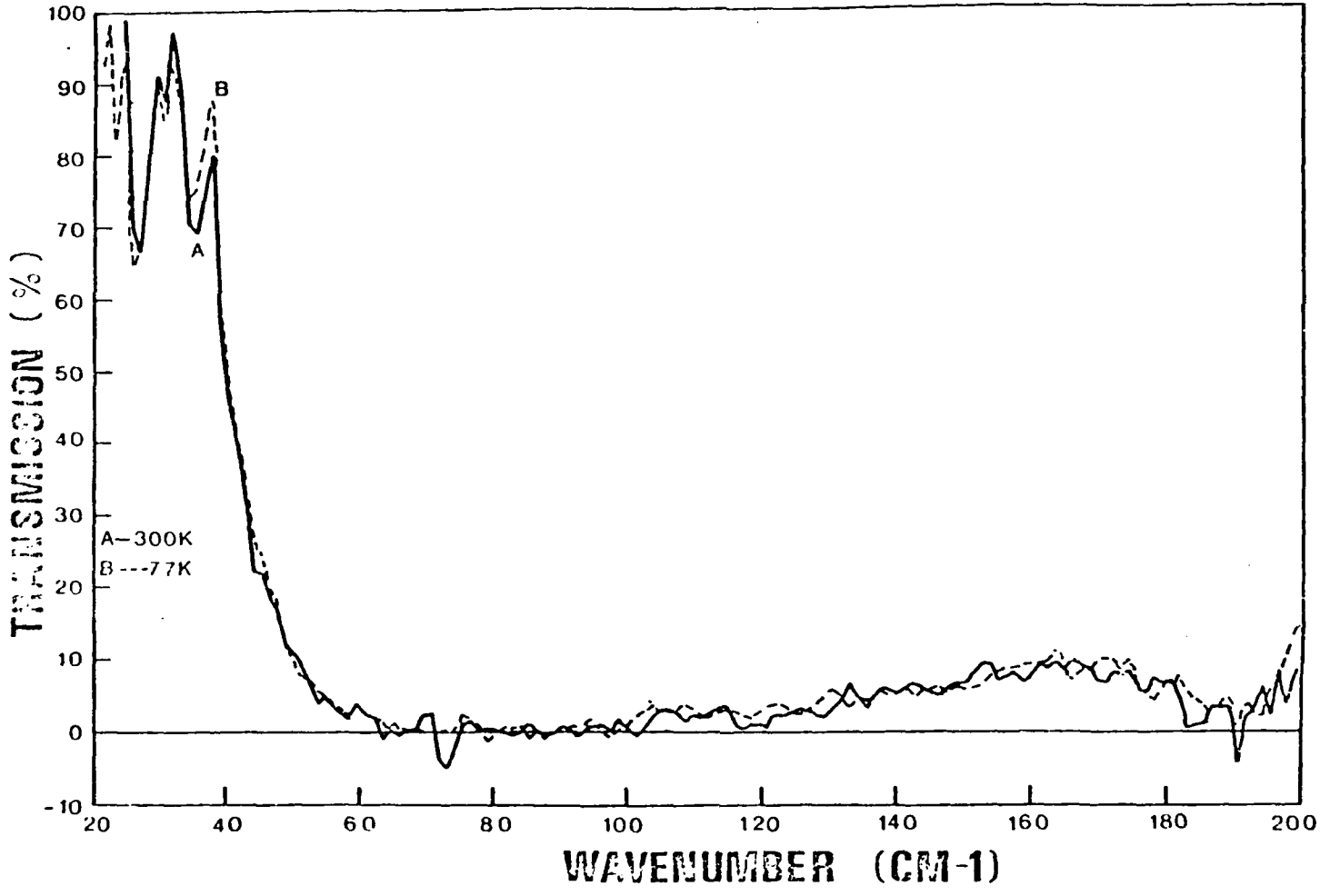

Fig. 4.8 Transmission profiles of Low Pass Filter: (A) at room temperature (300 K) and (B) at 77 K after repeated cycling from 300 K.

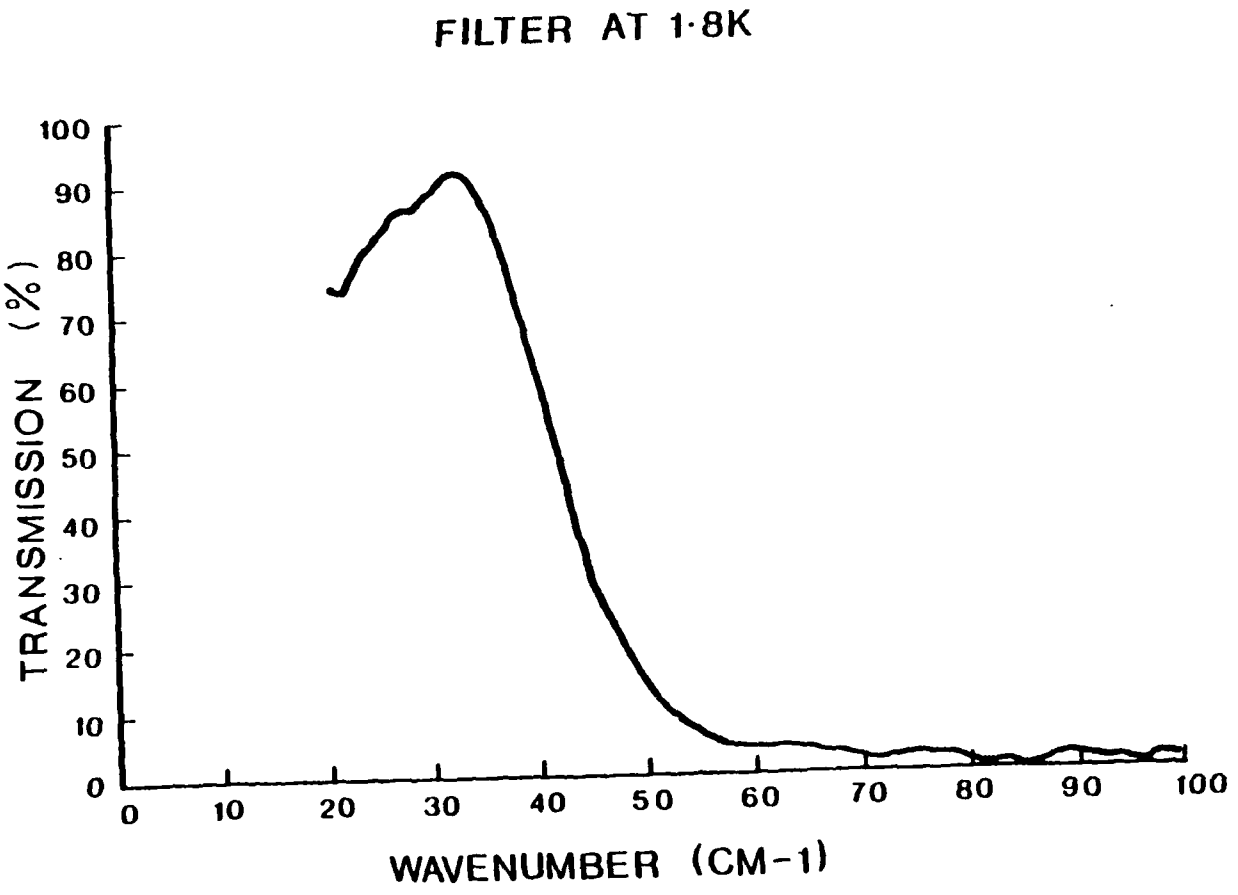

Fig. 4.9 Transmission profile of Low Pass Filter at 1.8 K after two cycles from 300 K.

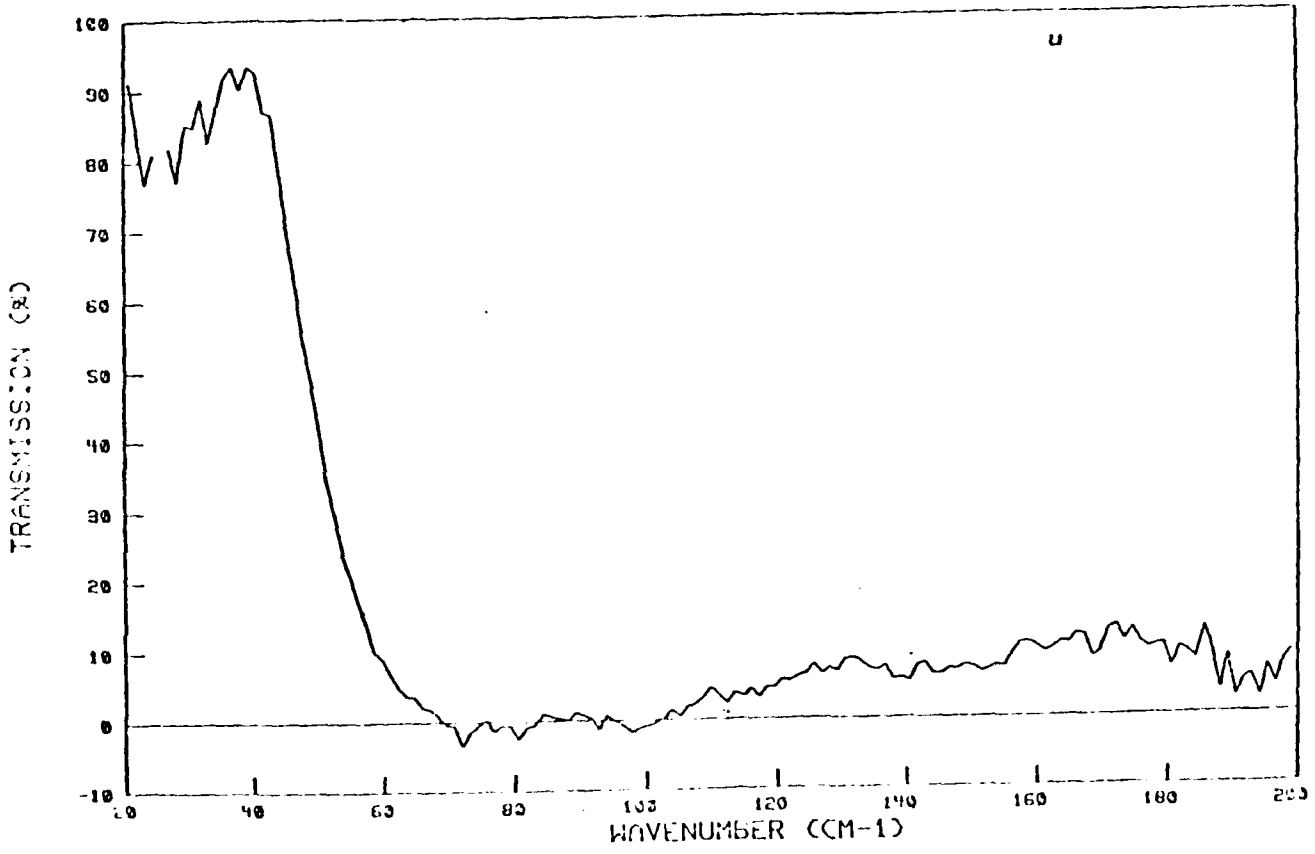

Fig 4.10 Low Pass Filter Profile.

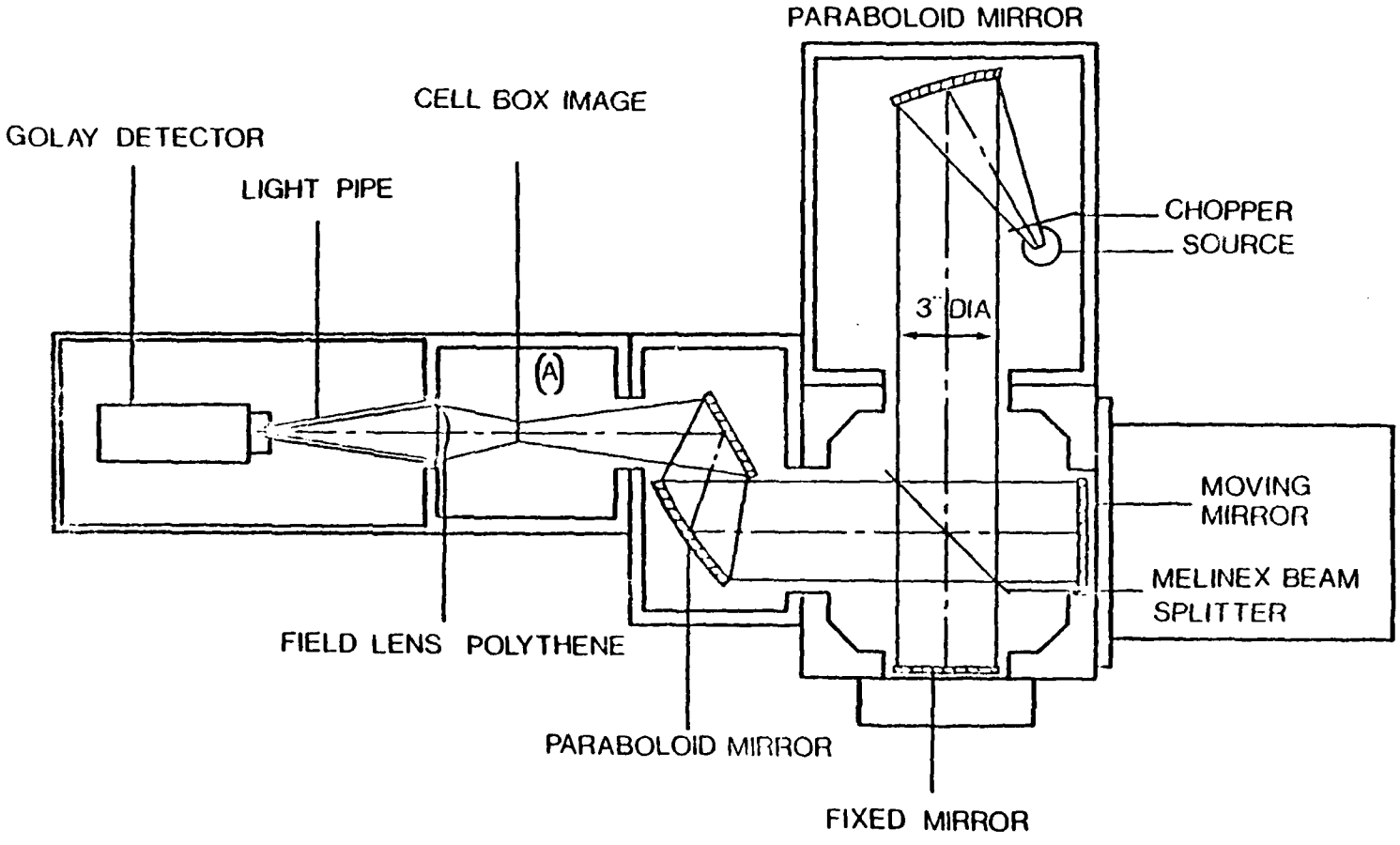

Fig. A1 Ray Diagram and optical layout of the Beckman RIIC FS720 interferometer.

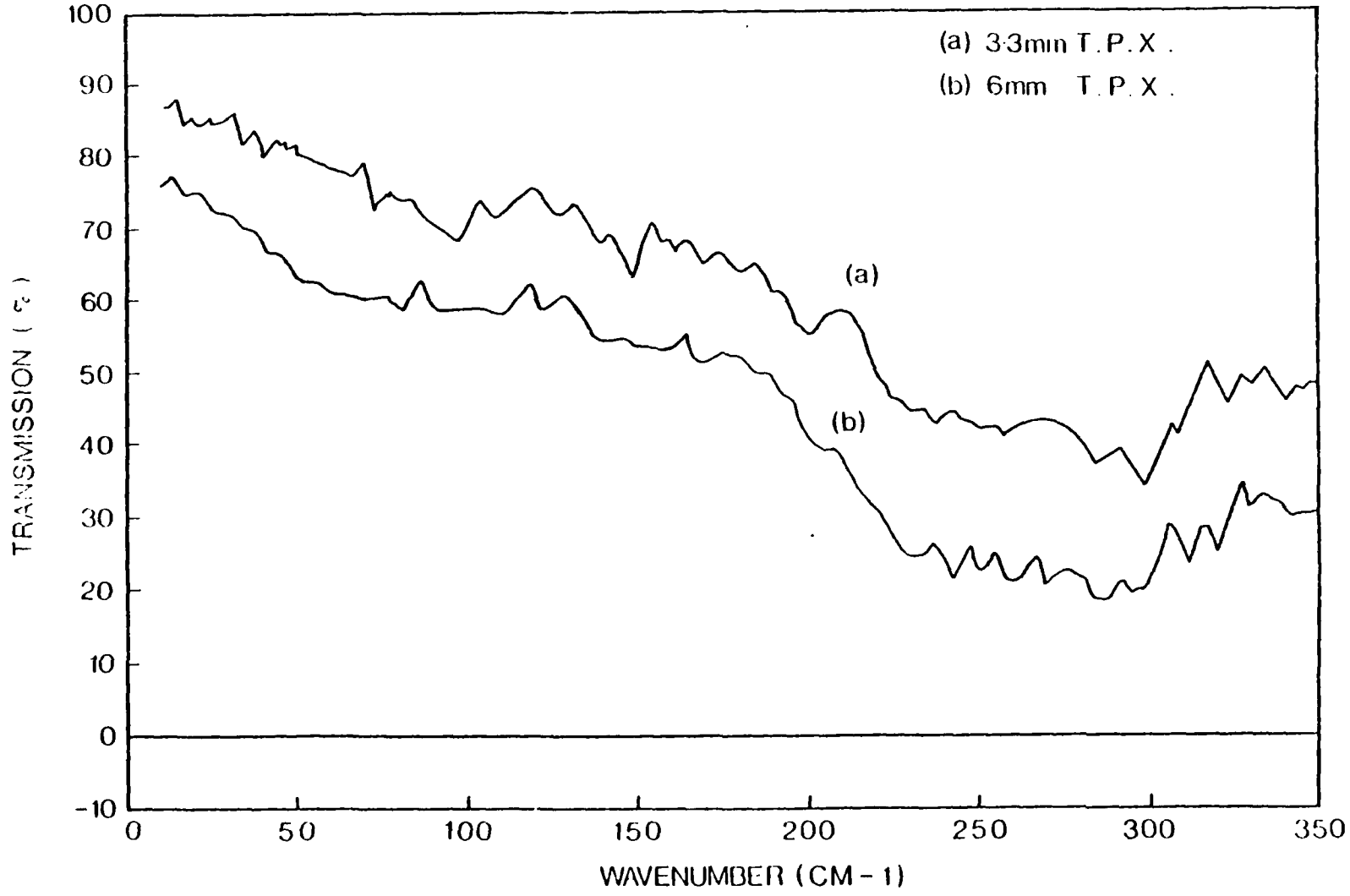

Fig A2 Transmission of (a) 3.3 mm and (b) 6 mm T.P.X.

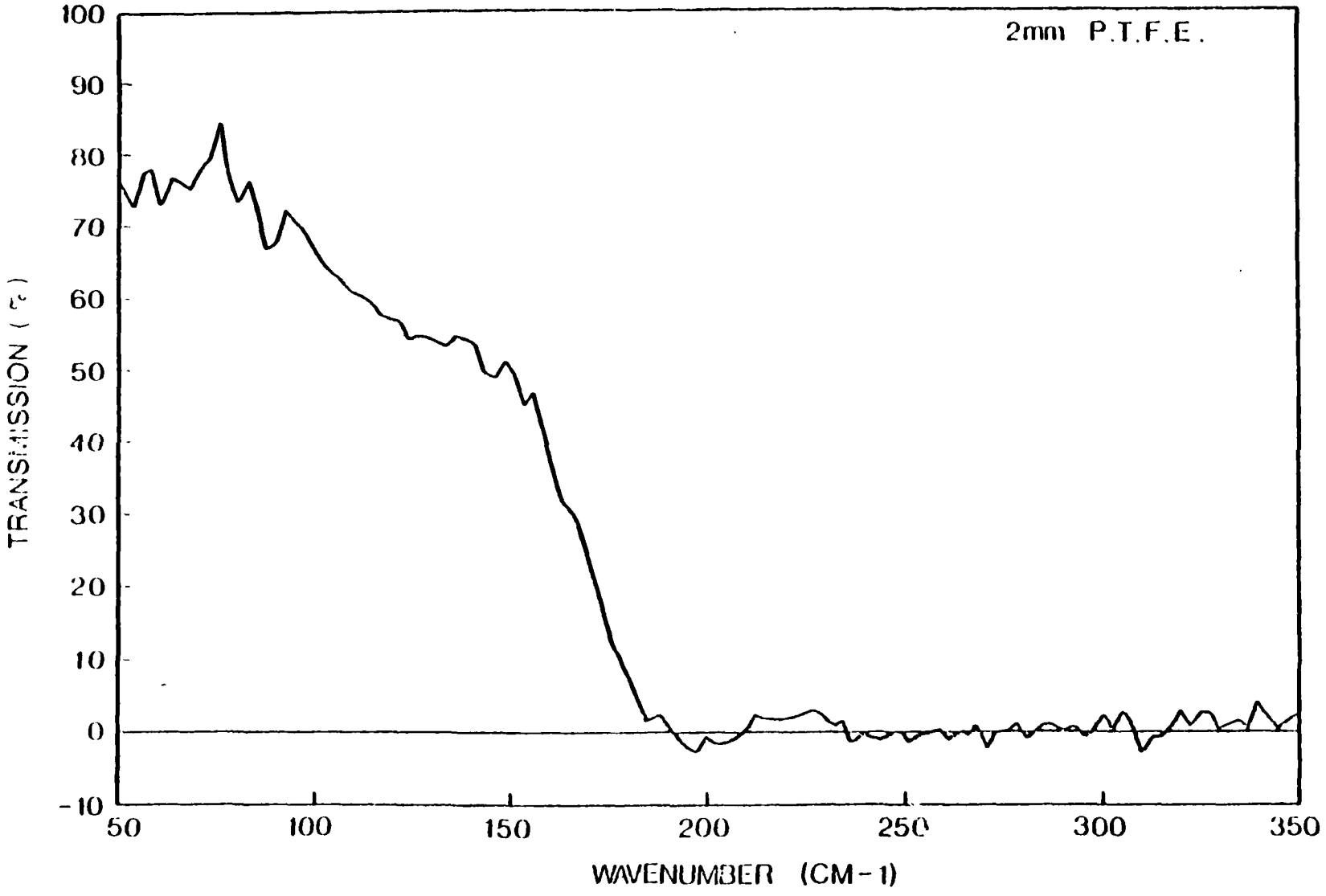

Fig.A3 Transmission of a 2 mm sample of P.T.F.E.

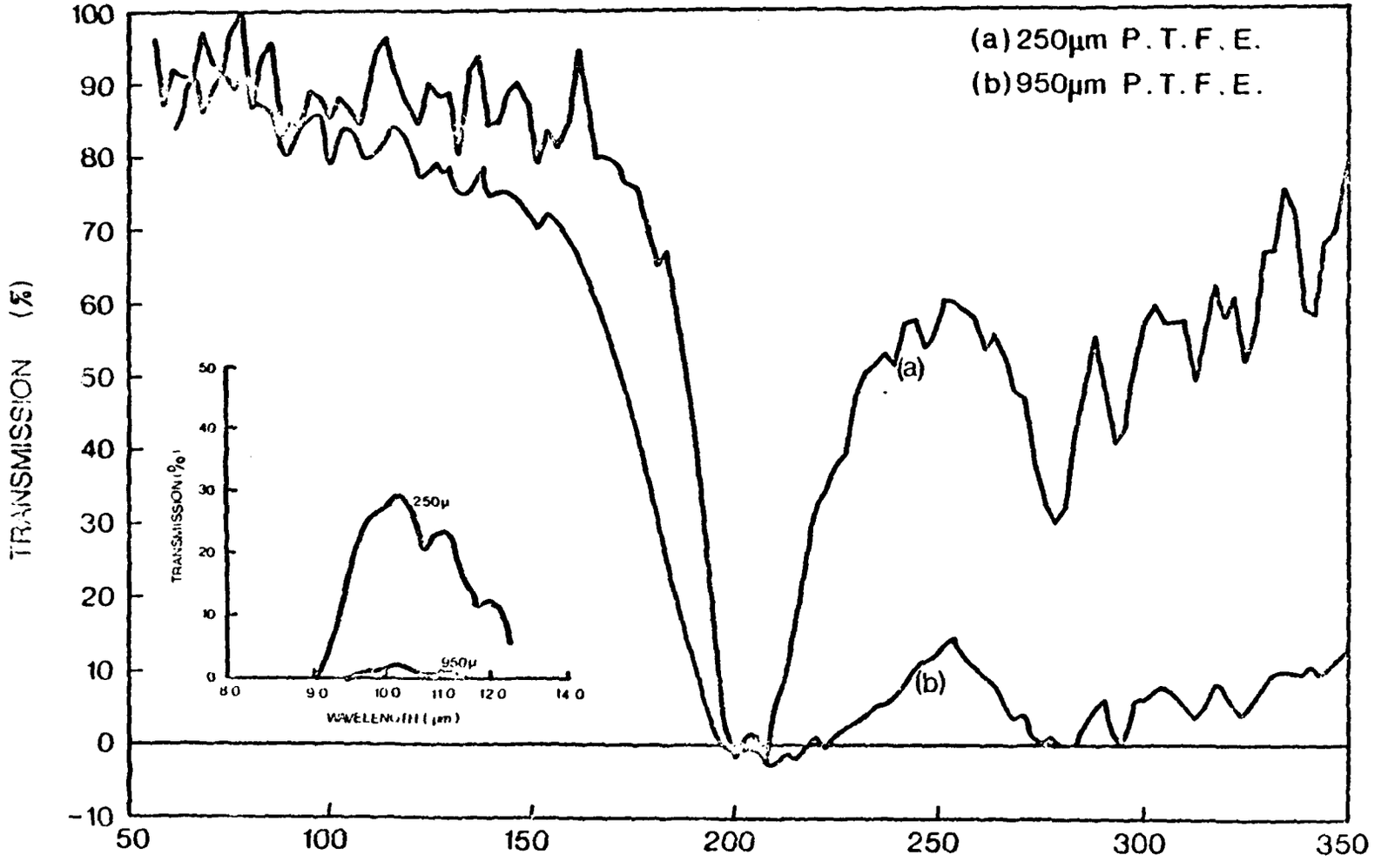

Fig.A4 I.R. and Subm. transmission curves for (a) 250 µm and (b) 950 µm P.T.F.E. (I.R. in insert).

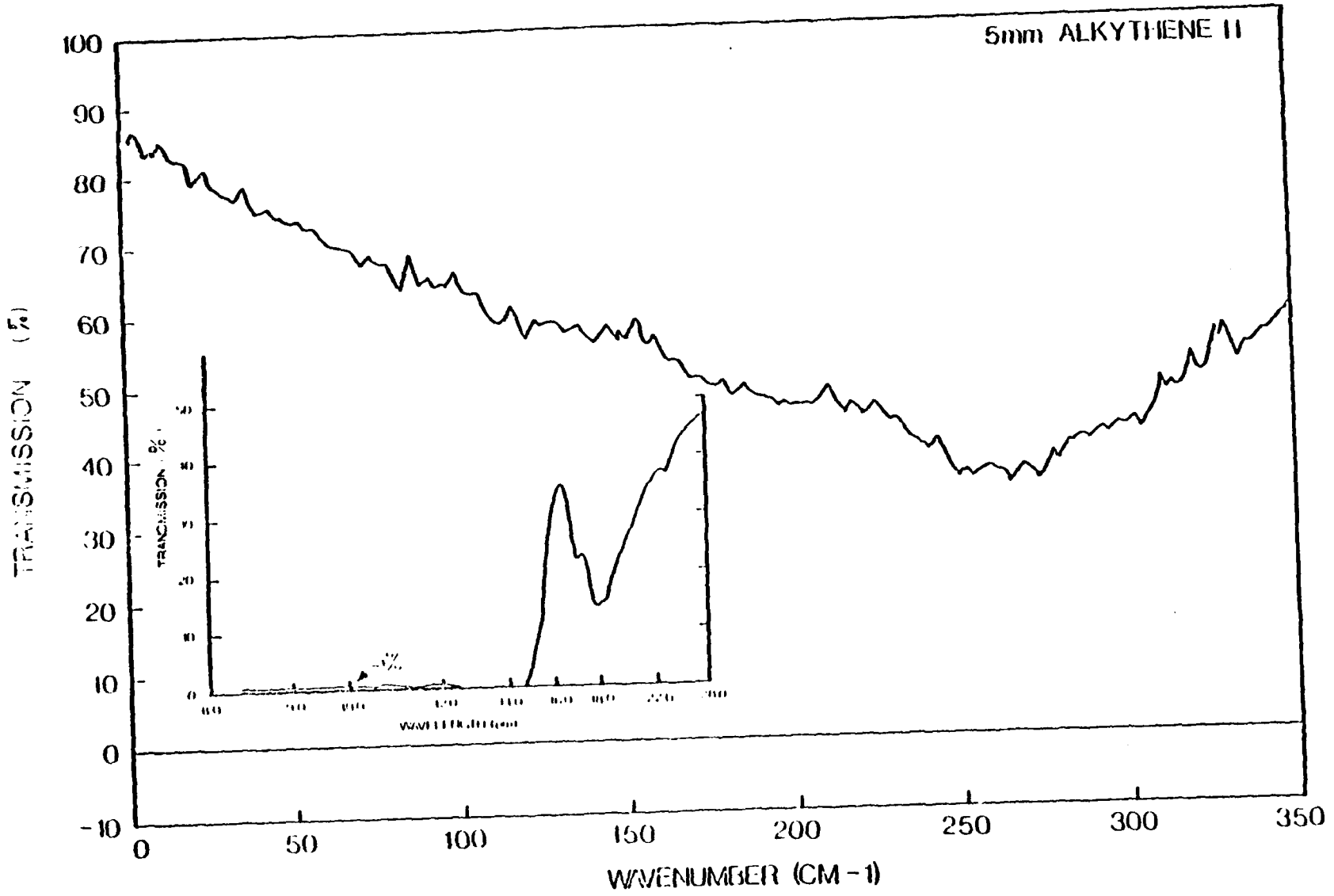

Fig.A5 I.R. and Subm. transmission curves for 5 mm Alkythene II (I.R. in insert)

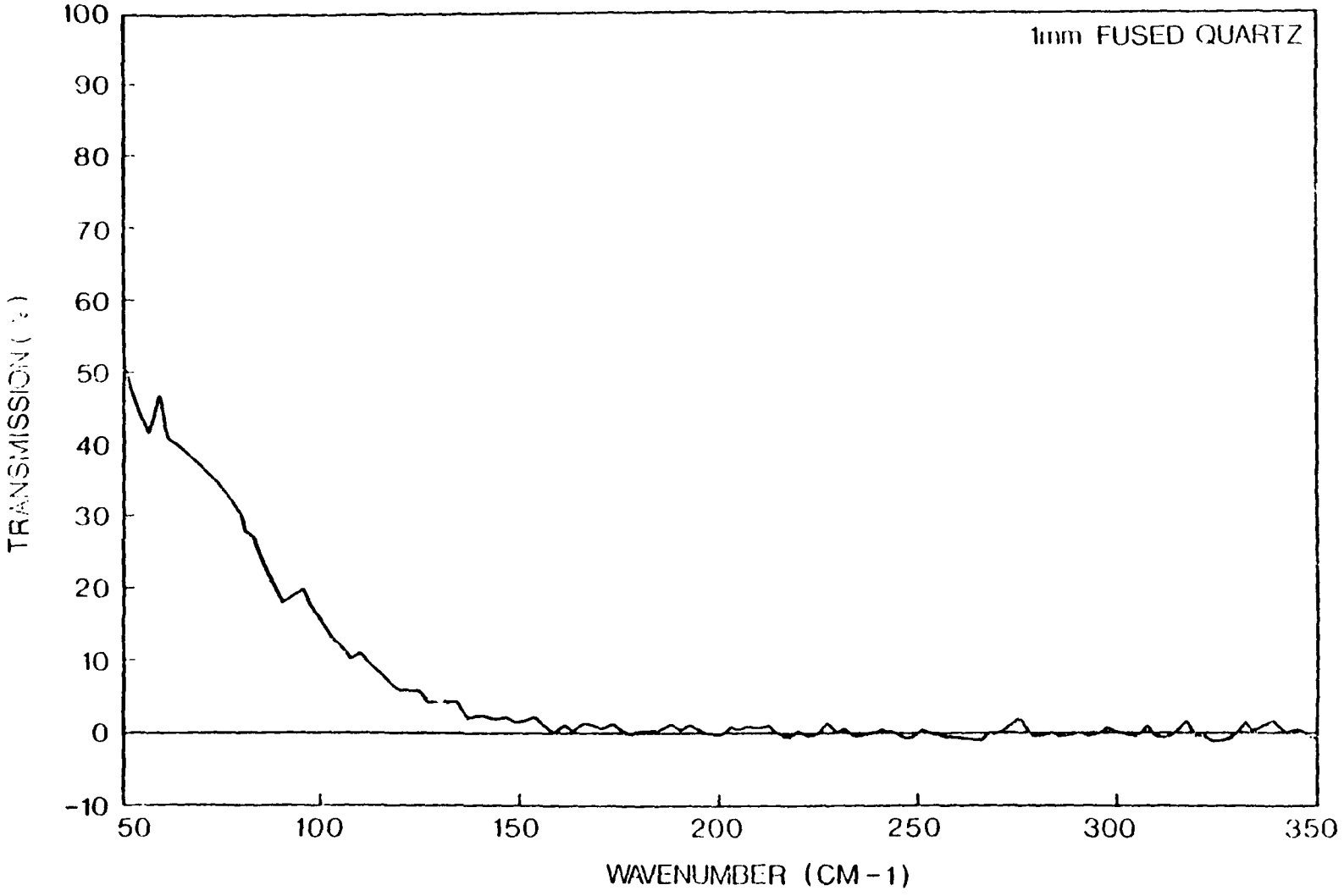

Fig. A6 Transmission of 1 mm Fused Quartz.

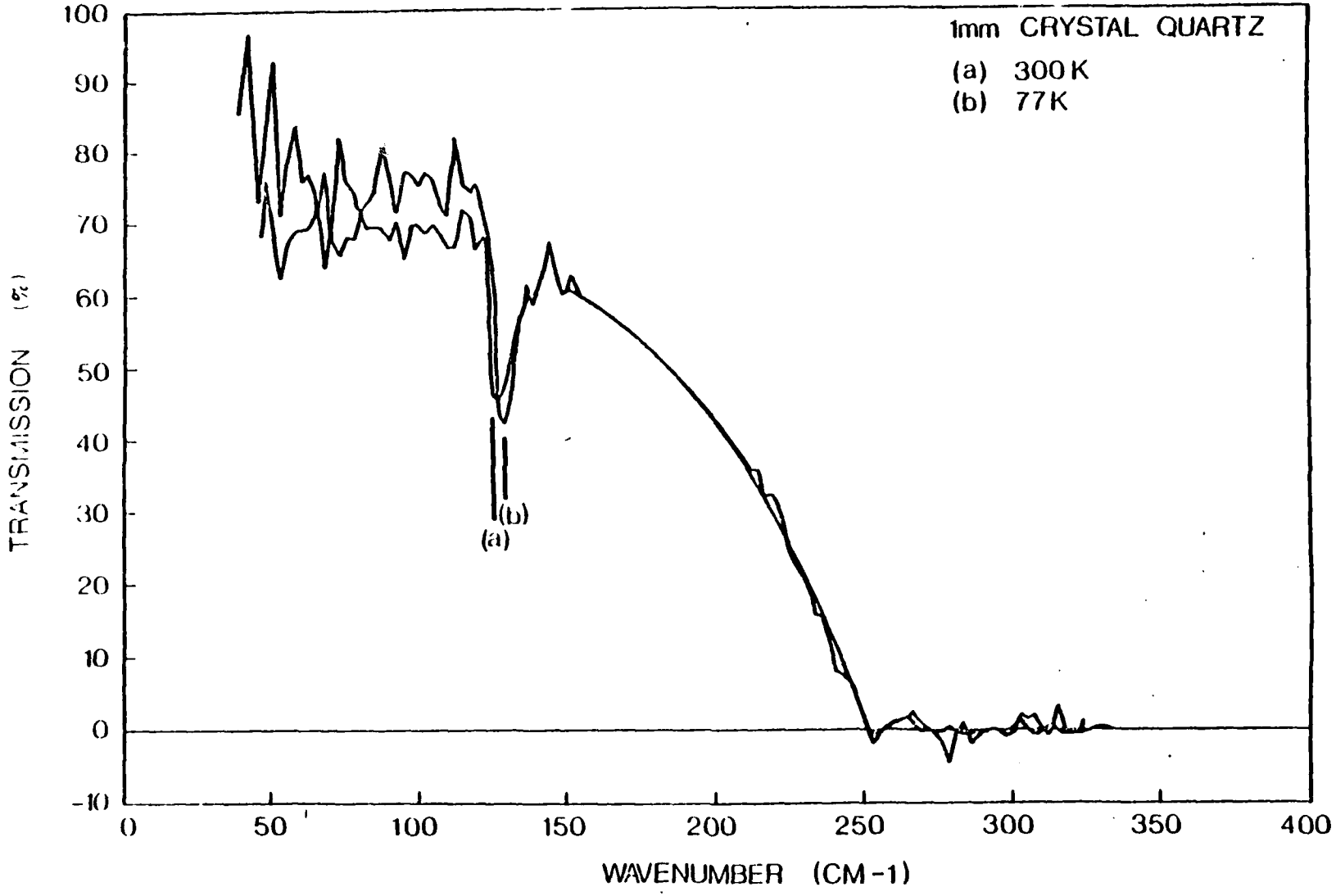

Fig.A7 Transmission curves for 1 mm Crystal Quartz at (a) 300 K and (b) 77 K.

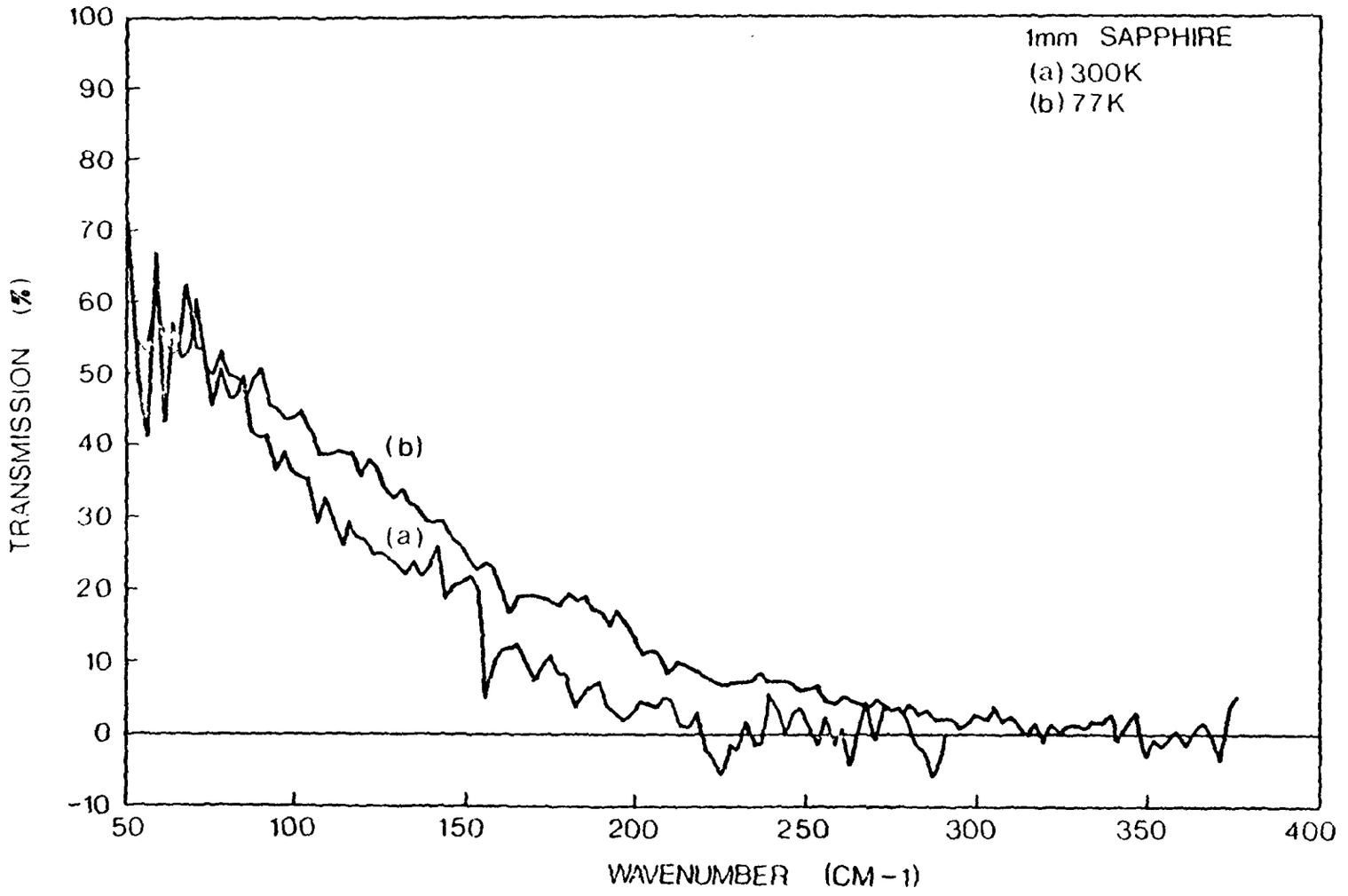

Fig.A8 Transmission curves for 1 mm Sapphire at (a) 300 K and (b) 77 K.

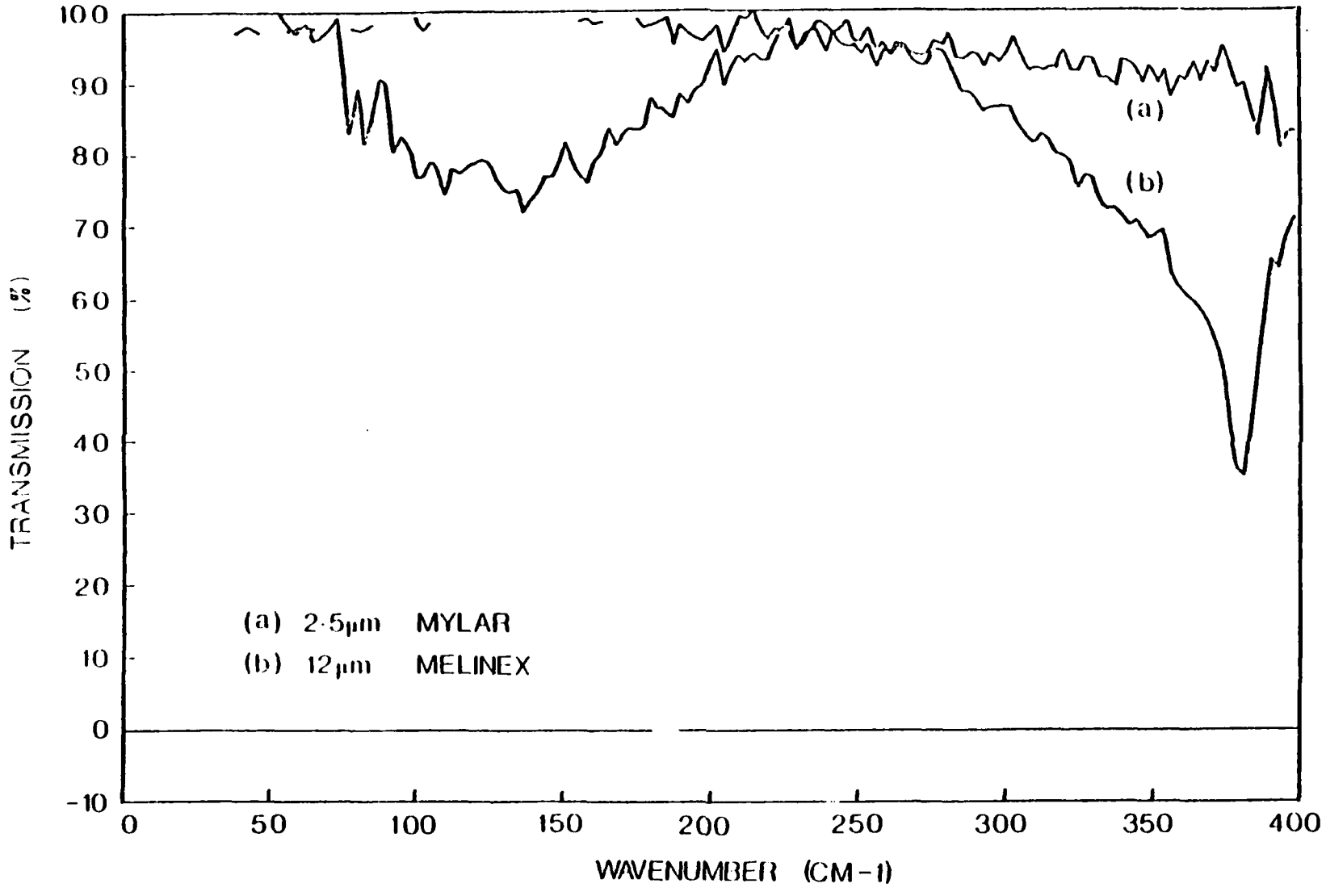

Fig.A9 Transmission of (a) 2.5 μm Mylar and (b) 12 μm Melinex.

LASER	MODE	CO_2 %	N_2 %	He %	H_2 %	X_e %
PL_3	Sealed	15.4	14.2	64.4	2	4
PL_3	Flowing	12	14	74	-	-
PL_4	Sealed	15.4	14.2	64.4	2	4
PL_4	Flowing	7	25	68	-	-

Table 1.1 Gas Mixes used in CO_2 Lasers.

Laser Gas	CO_2 line	Submillimetre λ (μm)	cw submillimetre power (mW)
CD_3OD	10R18	41	18.5
CH_3OH	9R18	65	0.93
$C_2H_4(OH)_2$	9P34	70.1	5.3
CH_3OH	9P34	70.6	5.3
CH_3OH	10R16	71	1.6
$C_2H_4(OH)_2$	9R10	95.8	4.2
CH_3OH	9R10	96.5	15.0
$C_2H_4(OH)_2$	9P36	118.0	15.9
CH_3OH	9P36	118.8	20.0
CH_3NH_2	9P24	148.5	0.9 *
CH_3OH	10R38	164	4.56 *
CH_3OH	9P36	170.6 (with blocking filter)	2
CH_3OH	9R18	186	3.2 *
CH_3OH	10R38	246	0.74
HCOOH	9R16	401	1.14
HCOOH	9R20	428	1.60 *
HCOOH	9R18	441	5.0 *
CH_3I	10P18	447	3.4 *
CH_3F	9P20	496	1.14 *
HCOOH	9R26	512	0.96 *
CH_3OH	9P16	570	5.64 *
CH_2CF_2	10P24	663	0.68 *
CH_2CF_2	10P22	890	0.40 *
$^{13}CH_3F$	9P32	1222	6.0 *
			* metal guide

Table 2.1 Submillimetre laser performance (with normal $^{12}C^{16}O_2$ pumping).

Molecule	Purity	Supplier
CD_3OD	99.0 atom % D	BOC, Prochem, London, UK
CH_3OD	99.0 atom % D	BOC, Prochem, London, UK
CD_3OH	99.0 atom % D	BOC, Prochem, London, UK
$^{15}NH_3$	99.3 atom % ^{15}N	BOC, Prochem, London, UK
NH_3	99.6% ^{14}N, 0.4% ^{15}N (Natural Isotopic Abundance)	Cambrian Chemicals, London, UK

Table 2.2 Molecules used to yield new submillimetre emissions.

$^{13}C^{16}O_2$ Laser Line	Pump Power (Watts)	Molecule	Wavelength (μm)	Power (mW)
10P24	13.7	$^{15}NH_3$	78.5 ± 0.3	2.3
9R28	6.25	CH_3OD	86.7 ± 0.3	11.6
10P18	15.5	$^{15}NH_3$	110.0 ± 0.3	8.4
10P14	16.2	$^{15}NH_3$	112.3 ± 0.3	11.6
10P14	13.5	NH_3	112.3 ± 0.3 (A)	5.0
10P24	14.5	NH_3	124.6 ± 0.3 (A)	2.5
9P18	13.9	CD_3OH	143.4 ± 0.3	2.6
10R18	17	NH_3	152.9 ± 0.3 (B)	9.8
9P14	8.5	CD_3OD	167.5 ± 0.3	2.6
9P12	6	CD_3OD	182.0 ± 0.5	5.2
9P36	6	CD_3OH	221.0 ± 0.3	0.44
9R34	10.5	CD_3OH	234.7 ± 0.3	1.0
9P16	10	CD_3OH	309.8 ± 0.5	1.3
9P16	13	CD_3OD	310.0 ± 0.5	2.6
9P18	10	CD_3OD	374.6 ± 0.5	0.20
10R10	13.2	$^{15}NH_3$	388.5 ± 0.5	1.3
10R10	13.7	NH_3	388.5 ± 0.5	7.8
9P20	11.2	CD_3OH	530.4 ± 0.5	0.9
9P20	7.5	CD_3OD	533.0 ± 0.5	0.12
9R24	11.25	CH_3OD	917 ± 3	0.3

Table 2.3 New cw submillimetre emissions resulting from $^{13}C^{16}O_2$ optical pumping.

$^{12}C^{16}O_2$ Laser Line	Pump Power (Watts)	Molecule	Wavelength (μm)	Power (mW)
10R34	27	CD_3OD	181.5 ± 0.5	0.16
10R16	37	CD_3OD	355.5 ± 0.5	13

Table 2.4 New cw submillimetre emissions resulting from $^{12}C^{16}O_2$ pumping.

No. of lines per inch (L.P.I.)	Metal	Effective g value (μm)	z_o^I	a/g
100	copper	285	1.1	0.22
150	copper	200	0.9	0.26
250	copper	116	1.0	0.24
400	nickel	74	1.4	0.15
500	copper	59	1.0	0.24
750	copper	40	0.65	0.35
750	nickel	40	0.75	0.31
1000	copper	29	0.575	0.38
1000	nickel	29	0.8	0.29
1000	copper	29	0.96	0.25
1270	copper	25	0.54	0.39
1500	copper	21	0.50	0.40

Table 4.1 Details of the available inductive meshes

No. of lines per inch (L.P.I.)	Metal	Effective g value (μm)
30	Aluminium	25
46	"	32.6
70	"	51
141	"	54
282	"	103
605	"	202
686	"	400
1016	"	597
1411	"	919

Table 4.2 Details of available capacitive mesh

MATERIAL	SUPPLIER
T.P.X.	Yarsley Technical Centre, Trowers Way, Redhill, Surrey, U.K.
P.T.F.E.	I.C.I. Ltd., Plastics Division, Welwyn Garden City, Herts, U.K.
Alkythene 11	I.C.I. Ltd., Plastics Division, Welwyn Garden City, Herts, U.K.
Mylar/Melenix	I.C.I. Ltd., Plastics Division, Welwyn Garden City, Herts, U.K.
Fused Quartz	Heraeus, 26 Albion Way, Kelvin Estate, East Kilbride, Glasgow G75 OYD.
Crystal Quartz	Specac Analytical Accessories Ltd., Unit 3, Lagoon Road, St. Mary Cray, Orpington, Kent, U.K.
Sapphire	Oriel Scientific Ltd., P.O. Box 136, Kingston-upon-Thames, Surrey, U.K.

Table A1 Suppliers of Materials Described.


DAT
FILM